THE ASTROPHYSICAL JOURNAL, 472:83–101, 1996 November 20

CIRCUMNUCLEAR STAR FORMATION IN ACTIVE GALAXIES

THAISA STORCHI-BERGMANN,[1] ALBERTO RODRÍGUEZ-ARDILA,[2] AND HENRIQUE R. SCHMITT[1,2,3]
Departamento de Astronomia, Instituto de Física, Universidade Federal Rio Grande do Sul, C.P. 15051, CEP 91501-970 Porto Alegre, RS, Brazil; thaisa@if.ufrgs.br
ANDREW S. WILSON[1,3]
Department of Astronomy, University of Maryland, College Park, MD 20742
AND
JACK A. BALDWIN
Cerro Tololo Inter-American Observatory, National Optical Astronomy Observatories, Casilla 603, La Serena, Chile
Received 1996 March 15; accepted 1996 June 13

ABSTRACT

We study the gas kinematics and chemical abundances in the inner regions of six galaxies with active galactic nuclei. The galaxies were selected for having star-forming regions in rings or spirals within a few kiloparsecs of the nucleus. The goal of the project is to search for any connections between the gas-dynamics, the chemical abundances, and the nuclear activity. Narrowband images have been obtained to map out the ionized gas. Medium-dispersion long-slit spectroscopy at several positions over the nuclear region has been used to obtain the gaseous velocity field and distribution of excitation. The H II regions in the rings are located near the turnover point of the rotation curves, suggesting association with the inner Lindblad resonance. The nuclear ring in the LINER NGC 1326 may be located between the two inner Lindblad resonances, and the inner rings in the Seyfert 2 galaxy NGC 3081 and the LINER/Seyfert 1 NGC 7213 may be associated with the $\Omega - \kappa/4$ resonance. A warm ionized medium (WIM) is found to pervade the inner region in all galaxies. There is a correlation between the [N II]/Hα and [S II]/Hα ratios and the FWHM of the [N II] λ6584 emission line in this WIM, indicating that shocks contribute to the ionization of the gas. We show that contamination by this diffuse emission increases the measured [N II]/Hα and [S II]/Hα ratios at H II regions close to the nuclei and thus may account, in part, for the systematically higher [N II]/Hα and [S II]/Hα found in the present work and by previous authors for near-nuclear H II regions compared with H II regions farther out in the disk of the galaxy. In the present paper, we correct for this contamination by interpolating the contribution of the WIM at the H II regions and subtracting it off. Oxygen and nitrogen abundances are obtained for 18 H II regions and are extrapolated to obtain the abundance of the nuclear gas, which is found to range from solar to 2 times solar for oxygen and from 2 to 4 times solar for nitrogen. Such values are similar to those observed in nonactive galaxies with the same luminosity and morphological type and do not support the idea that the central regions of active galaxies have undergone unusual chemical processing.

Subject headings: galaxies: abundances — galaxies: active — galaxies: ISM — galaxies: nuclei — galaxies: Seyfert — galaxies: stellar content

1. INTRODUCTION

We investigate the circumnuclear gasdynamics and chemical abundances of three Seyfert 2 galaxies and three LINERs with H II regions in rings or spirals close to the active nuclei. The motivation for this work is twofold: (1) to search for any dynamical evidence of transfer of material ("fuel") to the active nucleus, since previous works have shown that rings are quite common in galaxies with active nuclei (e.g., Simkin, Su, & Schwarz 1980; Wilson et al. 1991; Genzel et al. 1995), and (2) to investigate whether the nuclear gas has anomalous chemical abundances, following studies of the narrow-line regions (NLRs) of the active nuclei, which suggest enhanced nitrogen abundances for the gas (Storchi-Bergmann & Pastoriza 1989, 1990; Storchi-Bergmann 1991; Storchi-Bergmann, Wilson, & Baldwin 1992; Schmitt, Storchi-Bergmann, & Baldwin 1994). As the NLRs are potentially subject to various uncertain processes additional to nuclear photoionization, such as heating by shocks and cosmic rays, a more reliable procedure is to measure the chemical abundances in H II regions located as close as possible to the active nuclei, on the assumption that their abundances can be extrapolated to the nuclei proper.

We have already used this approach to study two LINER nuclei with nuclear rings of star formation, NGC 1097 and NGC 1672 (Storchi-Bergmann, Wilson, & Baldwin 1996, hereafter SWB). We found that the nuclear rings have velocities distinct from the ambient rotation curve and that their abundances of oxygen and nitrogen are supersolar but not clearly excessive compared to the nuclear regions of nonactive galaxies of similar morphological type and luminosity. In the present paper, we continue our study of active nuclei with circumnuclear star-forming regions through

[1] Visiting Astronomer, Cerro Tololo Inter-American Observatory, operated by the Association of Universities for Research in Astronomy, Inc., under contract with the National Science Foundation.
[2] CNPq Fellow.
[3] Space Telescope Science Institute, 3700 San Martin Drive, Baltimore, MD 21218.

similar observations of the Seyfert 2 galaxies IC 1816, NGC 1386, and NGC 3081 and the LINERs NGC 1326, NGC 1598, and NGC 7213. Narrowband images have been used to map out the ionized gas. Medium-dispersion long-slit spectroscopy covering the spectral region around Hα has been used to obtain the gaseous velocity field. As in the cases of NGC 1097 and NGC 1672, the high sensitivity of these spectra has allowed the detection of line emission from diffuse gas pervading the inner region of all the galaxies observed. Lastly, low-dispersion spectra in the range 3600–7000 Å have been obtained in order to derive the chemical abundances of the H II regions. Brief descriptions of the individual galaxies follow.

2. THE SAMPLE

IC 1816 is an Sab galaxy harboring a Seyfert 2 nucleus. An uncalibrated nuclear spectrum was presented by Maia et al. (1987), who observed this galaxy during a redshift survey of the southern skies. Inspection of the galaxy's image in the European Southern Observatory ESO/SERC J Sky Survey Schmidt films reveals a tight spiral structure.

NGC 1326 is an early-type barred spiral in the Fornax Cluster and a member of the sample of nuclear ring galaxies compiled by Buta & Crocker (1993). It was observed in the radio continuum and CO bands, near-infrared, and Hα by García-Barreto et al. (1991) and contains a LINER nucleus (Véron-Cetty & Véron 1986).

NGC 1386 is an Sa galaxy, also in the Fornax Cluster, and is one of the closest Seyfert galaxies. The excitation and kinematics of the circumnuclear gas were studied by Weaver, Wilson, & Baldwin (1991), who also presented Hα and red continuum images. The galaxy has two spiral arms at ~1 kpc from the nucleus. The stellar population in the nuclear region has been investigated by Storchi-Bergmann, Bica, & Pastoriza (1990).

NGC 1598 is an Sbc galaxy and a member of the trio that includes the "Carafe." Its most remarkable property is the presence of faint linear optical features (jets?) along the minor axis (Hawarden et al. 1979). The nuclear spectrum was studied by Phillips et al. (1984), who classified it as a LINER superposed on a continuum from hot stars. The galaxy has two spiral arms with several H II regions at a range of distances from the nucleus.

NGC 3081 is an S0/a galaxy with a Seyfert 2 nucleus studied by Véron (1981), Phillips, Charles, & Baldwin (1983), Whittle (1985), and Appenzeller & Östreicher (1988). Broadband images are given by Buta (1990), who concluded that the galaxy has three rings: nuclear, inner, and external. Narrowband Hα images are presented by Durret & Bergeron (1986) and Pogge (1989).

NGC 7213 is an S0 galaxy with a nuclear spectrum showing characteristics of both a Seyfert 1 nucleus, from the presence of broad Hα and X-ray emission, and a LINER, from the narrow emission line ratios (Filippenko & Halpern 1984). It shows a faint inner ring of H II regions.

Basic data on these galaxies are presented in Table 1.

3. OBSERVATIONS AND REDUCTIONS

CCD images of the galaxies NGC 1386, NGC 1598, NGC 3081, and NGC 7213 were obtained at the 1.5 m telescope of the Cerro Tololo Inter-American Observatory, through narrowband filters centered on the [O III] λ5007 and Hα + [N II] λλ6548, 6584 emission lines and adjacent continua. A journal of the observations is shown in Table 2.

Long-slit spectra were obtained by use of the 4 m telescope, Cassegrain spectrograph, and a CCD detector at the same observatory in 1991 November, 1992 May, and 1994 January. The position angles were selected to cover as many H II regions as possible. The slit width was 300 μm, corresponding to 2″ on the sky. Two gratings were used: one to provide a medium-to-high spectral resolution suitable for a kinematic study and another for obtaining low-resolution spectra for the study of the chemical abundances. The detector used in the observations of 1991 November and 1994 January was a Tek 1024 on the folded Schmidt camera while, in 1992 May, we used the Reticon detector on the blue air Schmidt camera. The attained spectral resolutions were approximately 8 Å for the low-resolution and about 2 Å for the medium-resolution spectra, as measured from the FWHM of the sky lines. A journal of the spectroscopic observations is shown in Table 3.

The images and spectra were reduced by following standard procedures in IRAF. The spectra were flux-calibrated by using standard stars. The Hα and [O III] images were obtained by subtracting the continuum contribution (off-band filter) from the on-band image, after scaling the corre-

TABLE 1

BASIC DATA[a]

Galaxy	Type	D (Mpc)[b]	M_B	i[c] (deg)	P.A. Major Axis (deg)	Scale (pc arcsec^{-1})
IC 1816	Sab	66.6[g]	−20.3	36	125	323
NGC 1326.....	RSBa[d]	16.9[e]	−19.7	48	77	82
NGC 1386.....	Sa[f]	16.9[e]	−19.0	68	25	82
NGC 1598.....	Sbc	65.5[g]	−20.2	58	123	318
NGC 3081.....	S0/a[h]	28.7[g]	−19.2	49	74	139
NGC 7213.....	S0	23.0[g]	−20.8	36	45	113

[a] From Lauberts & Valentijn 1989, except where indicated.
[b] $H_0 = 75$ km s^{-1} Mpc^{-1}
[c] From the apparent axial ratio, assuming a thin disk.
[d] Sandage & Tammann 1987.
[e] Adopted distance to the Fornax Cluster (Tully 1988, p. 29).
[f] Weaver et al. 1991.
[g] From the radial velocity obtained in the present paper, corrected to the centroid of the Local Group.
[h] Buta 1990.

TABLE 2

LOG OF OBSERVATIONS—IMAGES

Filter (Å/ΔÅ)	Exposure (s)	Scale (arcsec pixel^{-1})	Date	Comments
NGC 1326:				
6606/75	200	0.24	1994 Aug 9/10	Hα + [N II]
7193/780.....	100	0.24	1994 Aug 9/10	Continuum
NGC 1386:				
5037/44	600	0.434	1991 Oct 8/9	[O III] on-line
5400/100.....	600	0.434	1991 Oct 8/9	Continuum
6563/75	600	0.434	1991 Oct 8/9	Hα + [N II]
7099/82	600	0.434	1991 Oct 8/9	Continuum
NGC 1598:				
6680/100.....	300	0.24	1994 Aug 11/12	Hα + [N II]
7193/780.....	300	0.24	1994 Aug 11/12	Continuum
NGC 3081:				
5037/44	600	0.24	1992 Apr 8/9	[O III] on-line
6606/75	600	0.24	1992 Apr 8/9	Hα + [N II]
7099/82	600	0.24	1992 Apr 8/9	Continuum
NGC 7213:				
5037/44	600	0.434	1991 Oct 8/9	[O III] on-line
6606/75	600	0.434	1991 Oct 8/9	Hα + [N II]
7099/82	600	0.434	1991 Oct 8/9	Continuum

sponding off-band images, such that the average integrated counts for the field stars were the same in the on-band and off-band images.

4. RESULTS

4.1. *Images*

We show in Figure 1 contour plots of the red (7193 Å) continuum and the continuum-subtracted Hα images of NGC 1326. In the continuum image, the main structures observed are an outer ring with major axis at P.A. ≈ 90° and a bar at P.A. ≈ 20°. The continuum-subtracted Hα image shows emission from only the nuclear ring, which is elongated along P.A. ≈ 90° like the outer ring. The strongest Hα emission does not come from the nucleus but from the eastern part of the nuclear ring.

In Figure 2, we show contour plots of the 5400 Å continuum and the continuum-subtracted Hα and [O III] λ5007

TABLE 3

LOG OF SPECTROSCOPIC OBSERVATIONS

Range (Å)	P.A. (deg)	Exposure (s)	Scale (arcsec pixel^{-1})	Resolution (Å)	Date	Comments
IC 1816:						
6000–7000.....	90	1800	0.9	2.1	1992 May 29/30	Through nucleus
3400–7000.....	90	1800	0.9	8	1992 May 28/29	Through nucleus
NGC 1326:						
6200–7200.....	77	1800	0.8	2.3	1994 Jan 4/5	Through nucleus
6200–7200.....	77	1800	0.8	2.3	1994 Jan 4/5	4″.5 NW
6200–7200.....	77	1800	0.8	2.3	1994 Jan 4/5	4″.5 SE
3700–6800.....	77	1800	0.8	8	1994 Jan 5/6	Through nucleus
NGC 1386:						
6200–7200.....	169	2700	0.8	1.7	1991 Nov 1/2	Through nucleus
3700–6800.....	169	1800	0.8	8	1994 Jan 6/7	Through nucleus
NGC 1598:						
6200–7200.....	123	1800	0.8	1.7	1994 Jan 4/5	Through nucleus
3700–6800.....	123	1800	0.8	8	1994 Jan 5/6	Through nucleus
NGC 3081:						
6200–7000.....	72.5	1800	0.9	2.1	1992 May 29/30	Through nucleus
6200–7000.....	72.5	1800	0.9	2.1	1992 May 29/30	7″.3 NW
6200–7000.....	72.5	1800	0.9	2.1	1992 May 29/30	7″.3 SE
3400–7000.....	72.5	1800	0.9	8	1992 May 28/29	Through nucleus
NGC 7213:						
6200–7200.....	50	1200	0.8	1.7	1991 Nov 2/3	Through nucleus
6200–7200.....	50	1200	0.8	1.7	1991 Nov 2/3	24″ NW
6200–7200.....	50	1200	0.8	1.7	1991 Nov 2/3	24″ SE
6200–7200.....	50	600	0.8	1.7	1991 Nov 2/3	12″ NW
6200–7200.....	50	600	0.8	1.7	1991 Nov 2/3	12″ SE
3400–7000.....	50	1200	0.9	8	1992 May 29/30	Through nucleus[a]
3400–7000.....	50	1800	0.9	8	1992 May 29/30	24″ NW[a]

[a] Clouds during observation of flux standard.

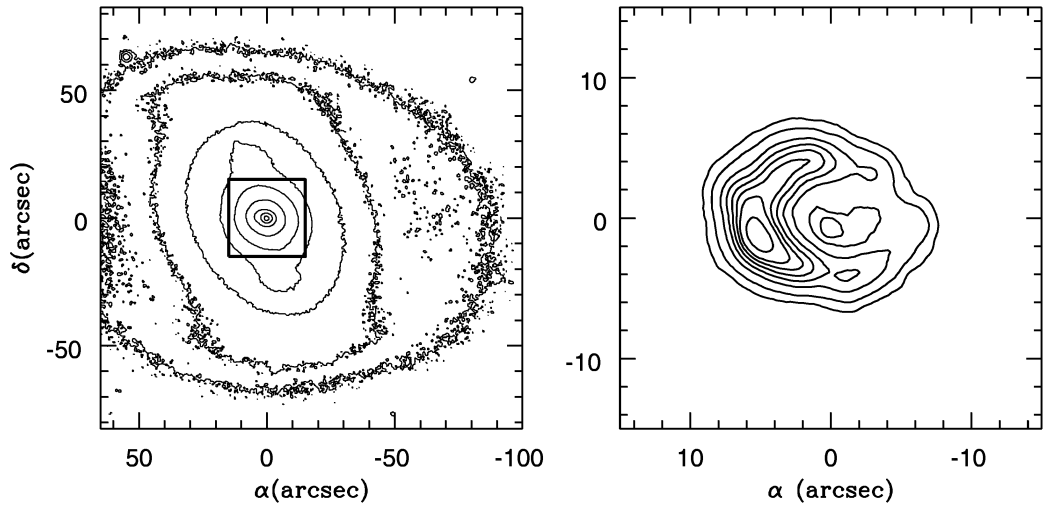

FIG. 1.—*Left*: Contour map of the red continuum image of NGC 1326, with levels at 1, 1.5, 2, 3, 5, 10, 30, 50, and 80 percent of the peak brightness above the sky. *Right*: Continuum-subtracted Hα image, with levels at 5, 10, 20, 30, 40, 50, 60, and 80 percent of peak brightness above the sky, enlarged to show details of the nuclear ring (there is no Hα emission outside the ring).

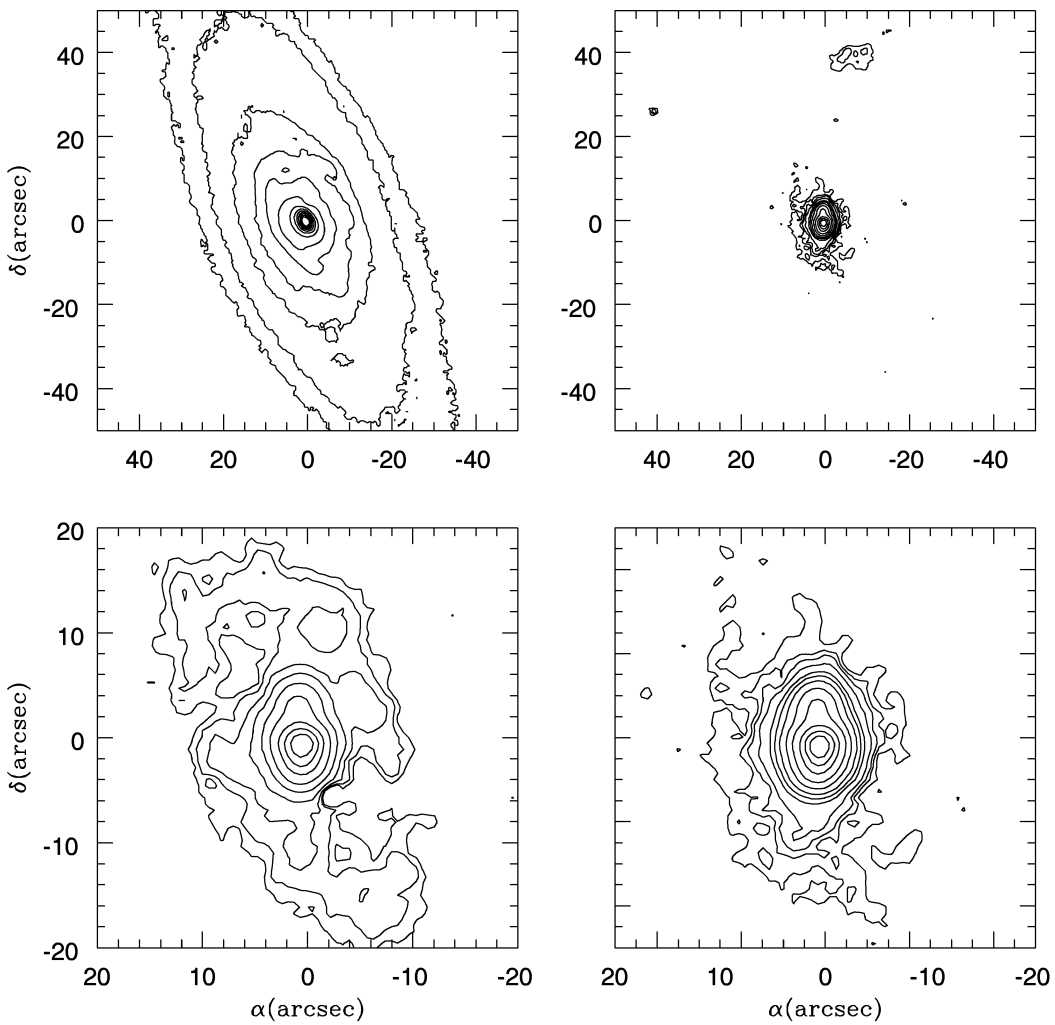

FIG. 2.—Contour maps of the NGC 1386 images. *Top left*: Red (5400 Å) continuum contoured at 0.5, 1, 2, 3, 5, 10, 20, 30, 40, 50, 60, 70, and 80 percent of the peak brightness above the sky. *Top right*: Continuum-subtracted [O III] λ5007 image, contoured at 0.2, 0.4, 0.6, 1, 2, 3, 5, 10, 20, 40, 60, and 80 percent of peak brightness, and showing a detached, off-nuclear region of high-excitation gas to the north. *Bottom left*: Continuum-subtracted Hα image, contoured at 1.5, 2, 3, 5, 10, 20, 40, 60, and 80 percent of the peak brightness. Note the change to a smaller scale to show details of the nuclear region. *Bottom right*: Same as top right, showing small-scale details of the nuclear region.

images of NGC 1386. The Hα image shows the two spiral arms previously reported by Weaver et al. (1991). Our continuum image is also similar to their red (7146 Å) continuum image. The [O III] image reveals an elongated structure extending ~10–20″ along the north-south direction, including a shoulder at ≈5″ north (0.4 kpc) from the nucleus, and a detached blob at ≈40″ north-northwest (3.3 kpc). The north-south elongation also shows up in the Hα image. The alignment of the inner contours with the detached blob is suggestive of nuclear ejection or anisotropic escape of ionizing radiation.

Figure 3 shows contour plots of the red (7193 Å) continuum and of the continuum-subtracted Hα image of NGC 1598. This latter image shows several H II regions along two spiral arms up to ~30″ (9.5 kpc) from the nucleus.

The red continuum (7099 Å) and the continuum-subtracted Hα and [O III] λ5007 images of NGC 3081 are shown in Figure 4. In the continuum image, the large-scale bar can be observed extending by ≈40″ along P.A. ≈ 66°, with the smaller "nuclear" bar extending ≈12″ along P.A. ≈ 120°. We do not observe, in the Hα image, any trace of a gaseous nuclear ring at the location of the blue nuclear ring found by Buta (1990) in continuum colors. Instead, both the Hα and the [O III] images show oval-shaped circumnuclear gaseous emission with major axis roughly perpendicular to the large-scale bar and extending by ≈10″. The inner ring can be seen in both the continuum and Hα image with the H II regions concentrated toward both ends of the large-scale bar.

Figure 5 shows the contours of the red continuum (7099 Å) and the continuum-subtracted Hα and [O III] images of NGC 7213. Note the smooth and symmetric appearance of the continuum image. The Hα image shows emission not only around the nucleus (extending for a few arcseconds) but also from a ring of H II regions at ≈20″ from the nucleus and a few H II regions outside the ring, suggesting the presence of partial spiral structure. The [O III] image shows emission at the nucleus and features in two patchy rings or a spiral (the spiral shape is more evident on the TV display). These ring features do not represent ionized gas, but rather reflect color variations over the galaxy that show up here because of the large wavelength difference between the on-band and off-band images (Table 2). Because no absolute flux calibration was taken, it is not possible to derive the true colors in the circumnuclear region. Rather, the ring features represent regions that are blue relative to their surroundings.

4.2. *Spectroscopy*

The medium-dispersion spectra were extracted from the two-dimensional frames by binning together 2 pixels (corresponding to approximately 2″ × 2″). The low-dispersion spectra were extracted by binning together 2 pixels in the nuclear region and the number necessary to cover the individual H II regions (typically 4–6 pixels) farther out. Emission lines were detected from the nucleus, neighboring locations, H II regions, and diffuse gas, and from high-excitation extranuclear regions in the case of NGC 1386.

In the following analysis, we have only used data for which the fluxes of the emission lines are larger than 2×10^{-16} ergs cm^{-2} s^{-1}, which corresponds to a 3–5 σ detection. In order to calculate the errors obtained on the gas kinematics, we have measured the spatial variation of the central wavelength and FWHM of the sky lines (as a function of distance from the center of the detector), as well as along the dispersion. Along the spatial direction, the peak wavelength of the sky lines varies by at most 0.4 Å from one extreme of the slit to the other. The FWHM of the sky lines increases toward the border of the detector by at most 0.3 Å. A difference of 0.3 Å was also found along the dispersion direction between the FWHM of a sky line near the central wavelength and lines near the limiting wavelengths of the spectral window. In the wavelength calibrations, the rms deviation of the fits was always smaller than 0.1 Å.

A sample of low-dispersion spectra is presented in Figures 6–11. For each galaxy, we show the spectra of the nucleus and of one or two H II regions. For NGC 1386, we also show the spectrum of the high-excitation blob 40″ northwest of the nucleus. The long-slit spectrum of this galaxy also shows [O III] emission from two other high-excitation blobs, at 54″ southeast and 69″ northwest. For NGC 7213, we also show the nuclear medium-dispersion

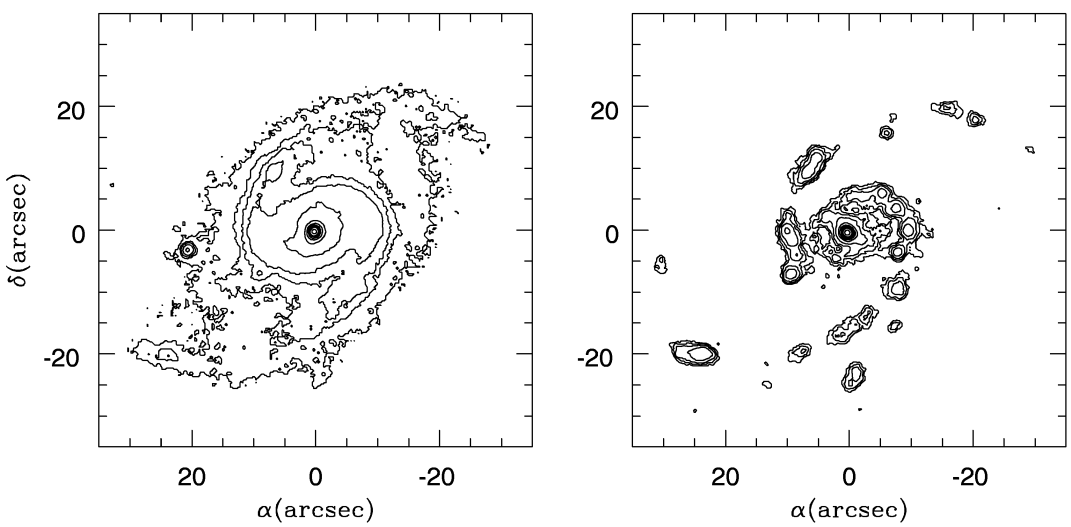

FIG. 3.—Contour maps of the NGC 1598 images. *Left*: Red continuum contoured at 1, 2, 3, 5, 10, 20, 30, 40, 50, 60, and 80 percent of peak brightness above the sky. *Right*: Continuum-subtracted Hα image, contoured at 2, 4, 6, 10, 20, 30, 40, 50, 60, and 80 percent of peak brightness.

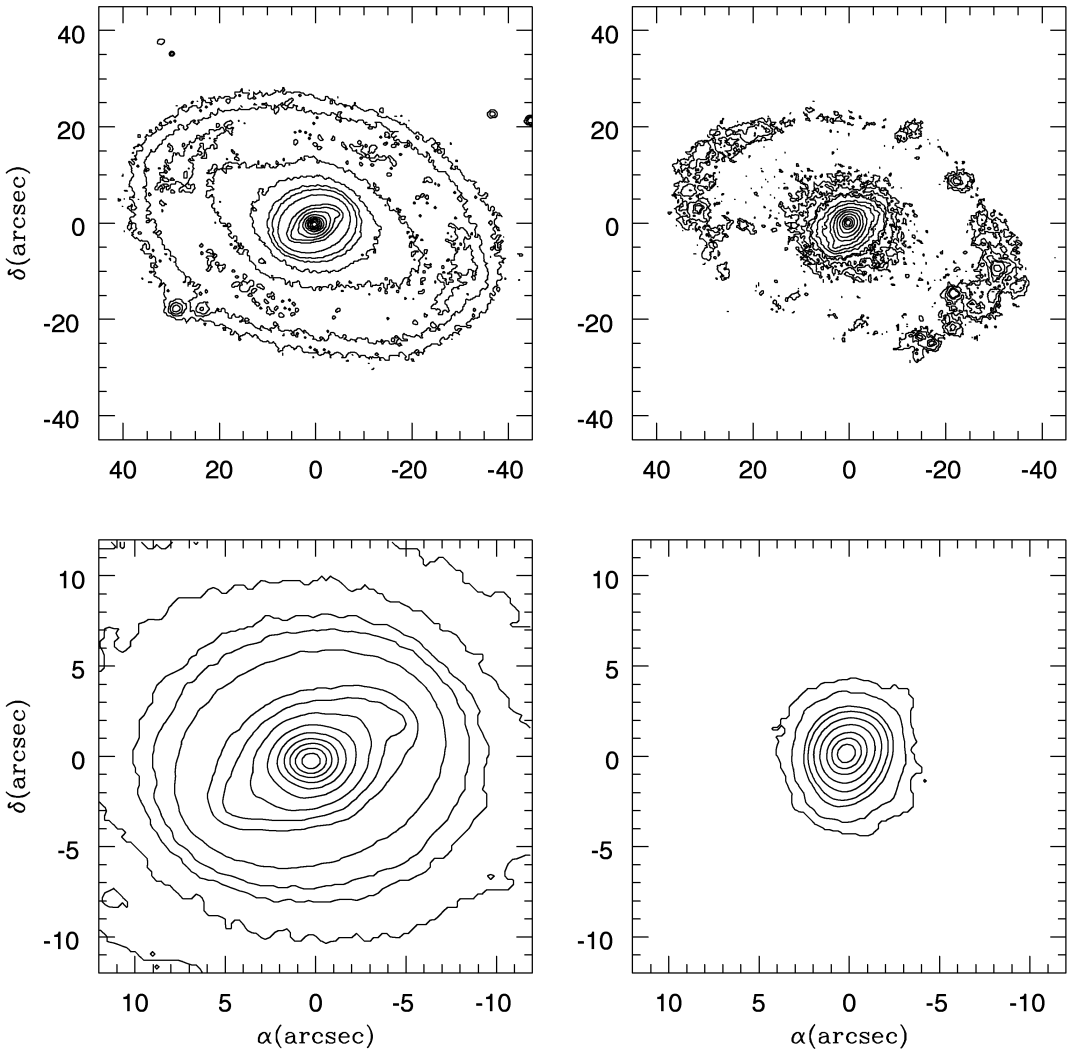

FIG. 4.—Contour maps of the NGC 3081 images. *Top left*: Red continuum contoured at 1, 1.5, 2.5, 3.5, 5, 7, 10, 20, 24, 30, 40, 50, 60, 70, 80, and 90 percent of the peak brightness above the sky. *Top right*: Continuum-subtracted Hα image, contoured at 0.5, 1, 1.5, 2.5, 4, 6, 10, 20, 40, 60, and 80 percent of peak brightness. *Bottom left*: Same as top left, enlarged to show details of the nuclear region. *Bottom right*: Continuum-subtracted [O III] λ5007 image, contoured at 0.5, 1, 3, 5, 10, 20, 40, 60, and 80 percent of peak brightness; emission is restricted to within 5″ of the nucleus.

spectrum, after subtraction of the stellar population obtained from a neighboring location in the bulge of the galaxy. We note that the broad Hα profile has changed as compared with the previous observations by Filippenko & Halpern (1984): the red shoulder has moved toward shorter wavelengths, and the blue shoulder, which was higher than the red, has disappeared. Analysis of the variation is beyond the scope of the present work.

5. GAS KINEMATICS

The medium-dispersion data were used to investigate the behavior of the gaseous velocity field. We analyze here the following sets of data: for the galaxies NGC 1326 and NGC 3081, we have long-slit spectra at three slit positions; for NGC 7213, we have spectra at five slit positions while, for IC 1816, NGC 1386, and NGC 1598, we have data at only one slit position. The peak wavelengths of Hα were used to obtain the velocities. From the measurements described above for the sky lines, we conclude that individual velocity measurements have uncertainties of $\approx$5–10 km s^{-1}, while the maximum systematic error between opposite ends of the slit is $\approx$20 km s^{-1}.

We show in Figures 12, 13, and 14 a representation of the velocity field of the first three galaxies above, after subtraction of the systemic velocity (see below and Table 4). The circles represent the velocities of the peak of Hα emission, with the radii of the circles being proportional to the magnitude of the velocity. Open symbols represent blueshifts and filled symbols redshifts. The rotation curves from the spectra through the nuclei of NGC 1326, NGC 3081, and NGC 7213 are shown in Figure 15. The rotation curves from the single spectra (through the nuclei) of NGC 1386, NGC 1598, and IC 1816 are shown in Figure 16.

In order to analyze the gaseous velocity fields, we have used the approach of SWB, fitting the following analytic expression to the rotation curve (Bertola et al. 1991):

$$V_{\rm rot}(r) = V_{\rm sys} + \frac{Ar}{(r^2 + C_0^2)^{p/2}}\,, \qquad (1)$$

where $V_{\rm sys}$ is the systemic velocity, A, C_0, and p are parameters, and r is the radius in the plane of the galaxy. The observed radial velocity at a position (R, Ψ), where R is the projected radial distance from the nucleus in the plane of the sky and Ψ is the corresponding position angle, is given

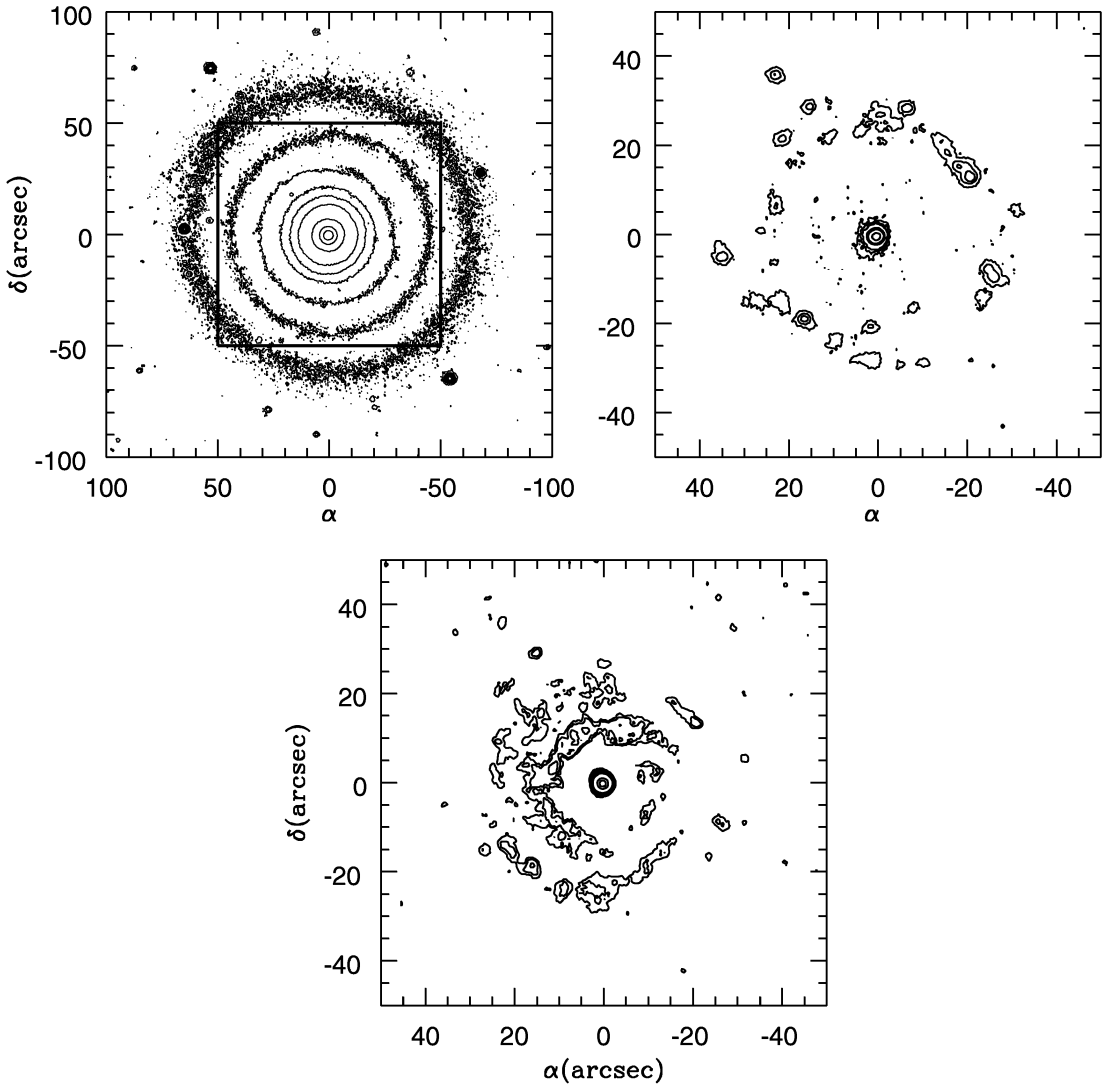

FIG. 5.—Contour maps of the NGC 7213 images. *Left*: Red continuum contoured at 0.25, 0.5, 1, 2, 3, 5, 10, 20, and 40 percent of peak brightness above the sky. *Right*: Continuum-subtracted Hα image, contoured at 0.2, 0.5, 1, 5, 10, and 50 percent of peak brightness. *Bottom*: [O III] λ5007 image after subtraction of the red continuum. The apparent emission in rings is not from ionized gas but an artifact of the strong continuum color variations (see § 4.1).

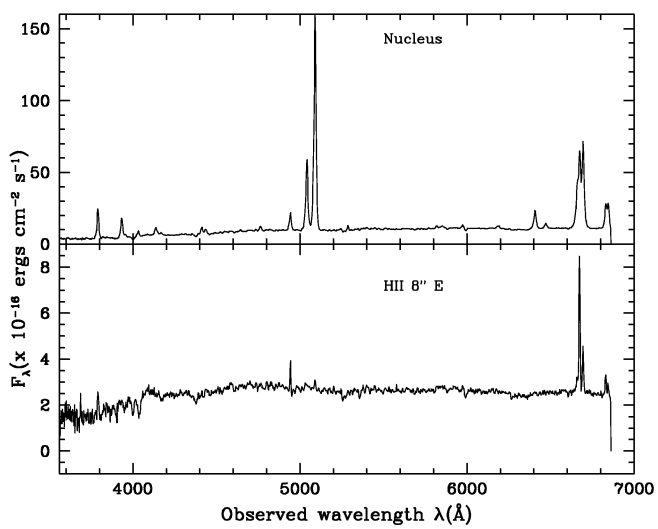

FIG. 6.—Spectra of the nucleus (*top*) and of an H II region at 8″ east from the nucleus (*bottom*) of IC 1816.

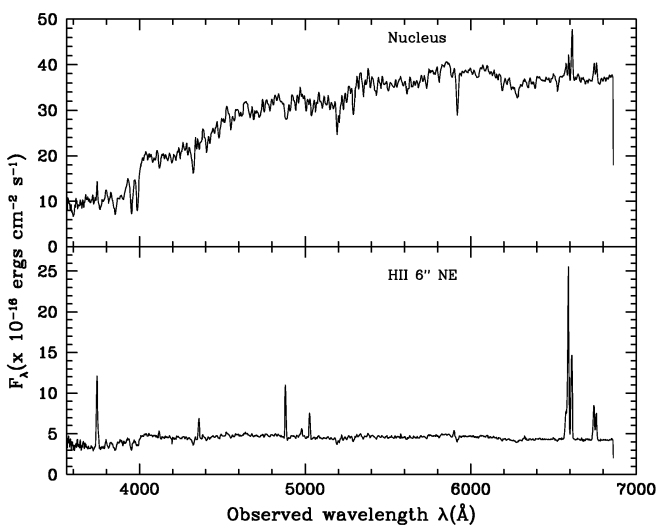

FIG. 7.—Spectra of the nucleus (*top*) and ring at 6″ northeast from the nucleus (*bottom*) of NGC 1326.

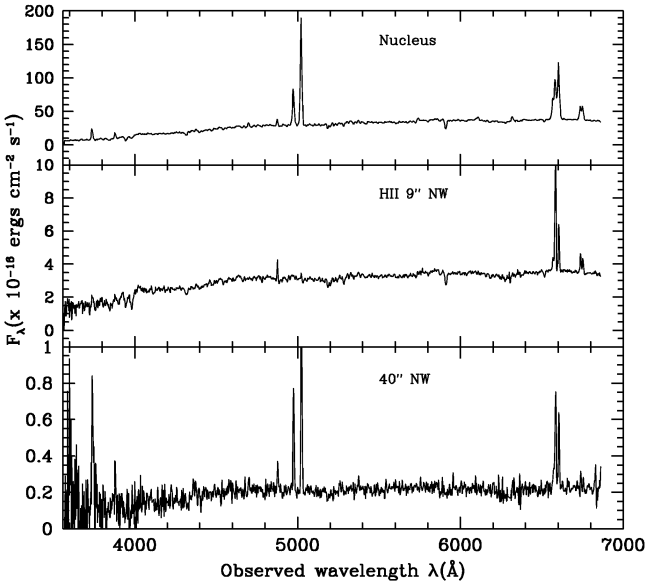

FIG. 8.—Sample spectra of NGC 1386. *Top to bottom*: Nucleus, H II region 9″ northwest of nucleus, and the high-excitation blob at 40″ northwest of the nucleus.

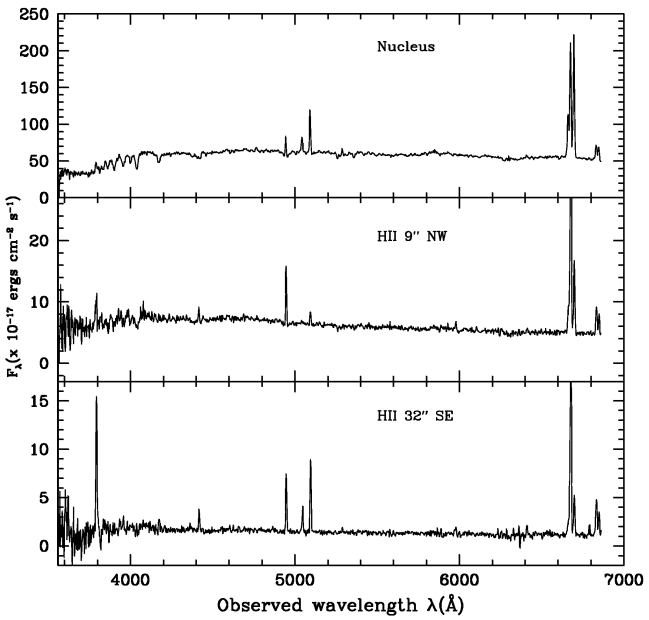

FIG. 9.—Sample spectra of NGC 1598. *Top to bottom*: Nucleus and H II regions at 9″ northwest and 32″ southeast of nucleus.

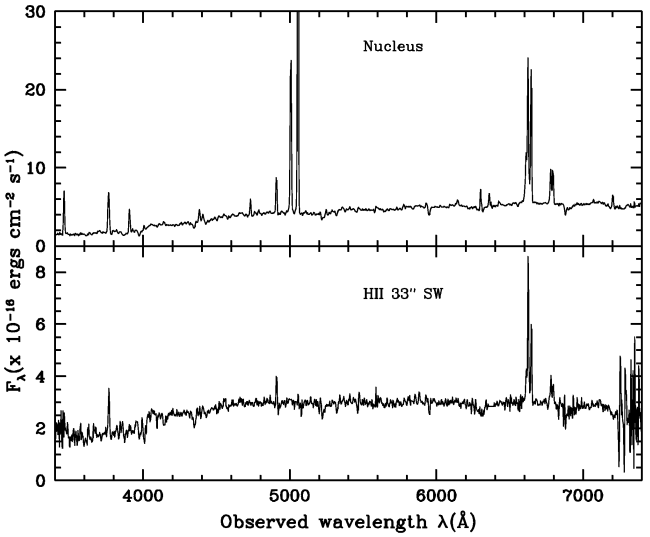

FIG. 10.—Spectra of the nucleus (*top*) and of an H II region at 33″ southwest from the nucleus of NGC 3081.

by

$$V_{\rm mod}(R, \Psi) = V_{\rm sys} + \frac{AR \cos(\Psi - \Psi_0) \sin i \cos^p i}{(R^2\xi + C_0^2 \cos^2 i)^{p/2}}, \quad (2)$$

where

$$\xi \equiv \sin^2(\Psi - \Psi_0) + \cos^2 i \cos^2(\Psi - \Psi_0),$$

i is the inclination of the disk ($i = 0$ for a face-on disk), and Ψ_0 is the position angle of the line of nodes.

For the three galaxies with data at more than one slit position, we determined the various parameters simultaneously by minimizing the residuals $\Delta V = V_{\rm obs} - V_{\rm mod}$, where $V_{\rm obs}(R, \Psi)$ is the observed radial velocity at position (R, Ψ) in the plane of the sky. We fitted the model to the observed velocity field by means of a nonlinear least-squares (Levenberg-Marquardt) algorithm, in which initial guesses must be given for the parameters.

Convergence was only obtained when the inclination was fixed at the photometric value (Table 1). In addition, for NGC 7213, we had to exclude from the fit a few points close to the nucleus, which did not follow equation (1), and also fix $p = 1$.

For IC 1816, NGC 1386, and NGC 1598, we have data along only one slit position. It was thus not possible to derive the position angle of the line of nodes, or the inclina-

TABLE 4

KINEMATIC PARAMETERS

Galaxy	$V_{\rm sys}$[a] (km s^{-1})	Ψ_0 (deg)	i (deg)	A (km s^{-1})	C_0 (kpc)	p
IC 1816	5080 ± 6	125[b]	36[b]	108 ± 9	1.89 ± 0.55	1.00[c]
NGC 1326.....	1374 ± 11	81 ± 3	48[b]	176 ± 10	0.30 ± 0.02	1.18 ± 0.06
NGC 1386.....	868 ± 5	25[b]	68[b]	187 ± 7	0.11 ± 0.07	0.99 ± 0.02
NGC 1598.....	5132 ± 5	123[b]	58[b]	141 ± 34	1.55 ± 0.40	1.06 ± 0.05
NGC 3081.....	2385 ± 7	107 ± 1	49[b]	222 ± 20	3.04 ± 0.30	0.98 ± 0.02
NGC 7213.....	1767 ± 10	20 ± 1	36[b]	223 ± 20	0.84 ± 0.5	1.00[c]

[a] Heliocentric.
[b] Photometric values.
[c] Adopted.

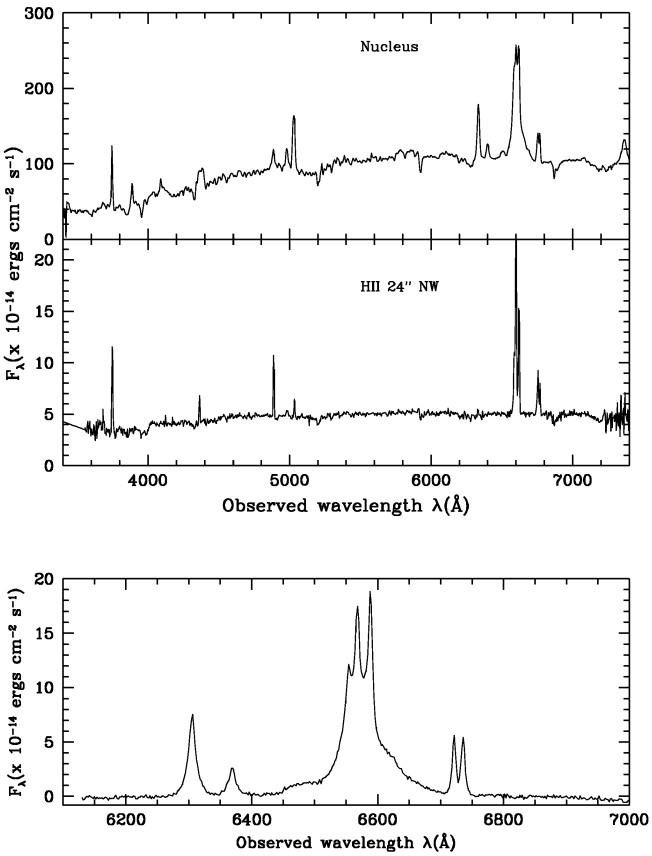

FIG. 11.—*Top to bottom*: Spectra of the nucleus and of an H II region 24″ northwest of the nucleus of NGC 7213, and a medium-resolution spectrum of the nucleus, after subtraction of the stellar population.

tion of the galaxy, from the kinematic data. We thus adopted the photometric values for Ψ_0 and i from Table 1.

The kinematic parameters obtained from the model fits to the rotation curves are presented in Table 4, where the values of V_{sys} have been corrected for Earth's orbital motion and are thus heliocentric. In order to judge the quality of the fits, we also show in the right panels of Figures 12, 13, and 14 the residuals (the difference between the observed velocity and model) for NGC 1326, NGC 3081, and NGC 7213. In Figure 15, we plot the models together with the data along the slit position crossing the nucleus for the three galaxies above, while Figure 16 shows the models for the other three galaxies together with the data along the single slit position.

The models represent well the gas velocities for NGC 1326 and NGC 3081, as the residuals are on average ≤ 10 km s^{-1} (only in a few locations do the residuals reach ≈ 20–30 km s^{-1}). For NGC 7213, there are locations where the residuals are larger (Fig. 14). Some 14″ south of the nucleus, there are residual blueshifts up to approximately 100 km s^{-1} while, at the same distance north, similar residual redshifts are found. The innermost locations along the slit crossing the nucleus also show large systematic residuals. The symmetric location of the large velocity residuals with respect to the nucleus is interesting and could be indicative of collimated outflow or other noncircular motions. More observations would be necessary in order to check such a pattern.

By comparing the velocity amplitudes derived from the model fits with those of normal galaxies with similar absolute magnitudes and Hubble types (Rubin et al. 1985), it can be concluded that the amplitudes are typical except for IC 1816, for which it is approximately 30%–40% smaller. However, little weight can be given to this discrepancy, as we have data only along one slit position for this galaxy. The parameter C_0, which is the radius at which the velocity reaches 70% of its amplitude, is also typical (≥ 1 kpc) except for NGC 1326 (0.30 ± 0.02 kpc) and NGC 1386 (0.11 ± 0.07 kpc), indicating large central mass concentrations in these two galaxies.

Our results for NGC 1386 can be compared with those from Weaver et al. (1991). Our gas velocity at the nucleus (defined as the peak of continuum light) is blueshifted by 67

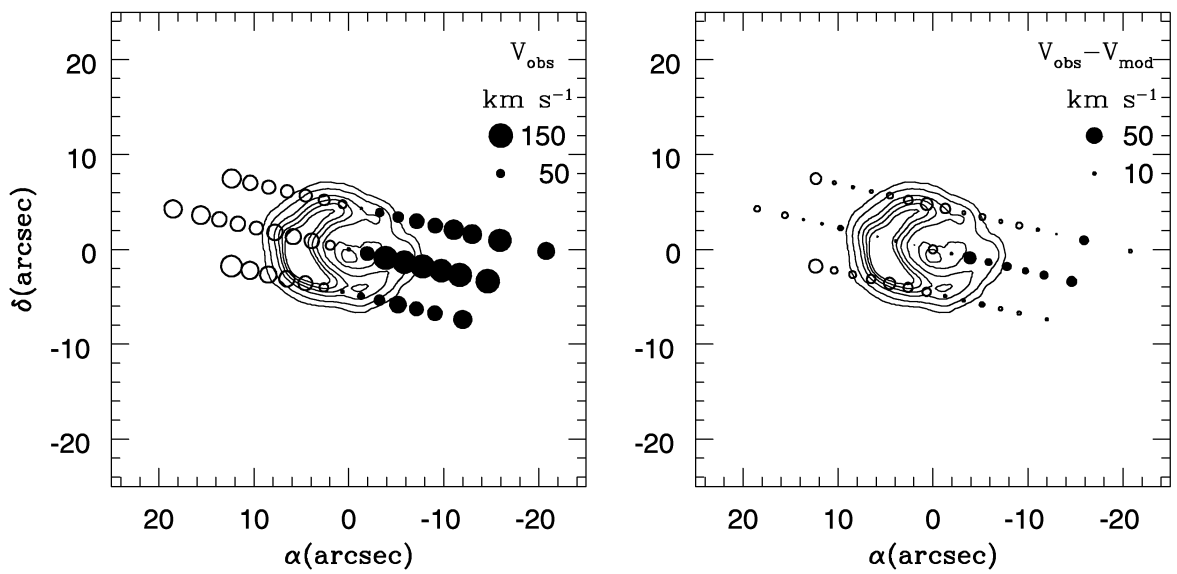

FIG. 12.—Velocity field of NGC 1326. *Left*: Circles represent the peak Hα velocities (after subtraction of the systemic velocity) superposed on the continuum-subtracted Hα image, with the radii of the circles being proportional to the magnitude of the velocity. Open circles represent blueshifts, filled circles redshifts. *Right*: Residuals between the measured velocity field and the model described in § 5. Errors in the individual velocity measurements range from 5 km s^{-1} (for the innermost locations) to ~ 15 km s^{-1} (for the outermost locations).

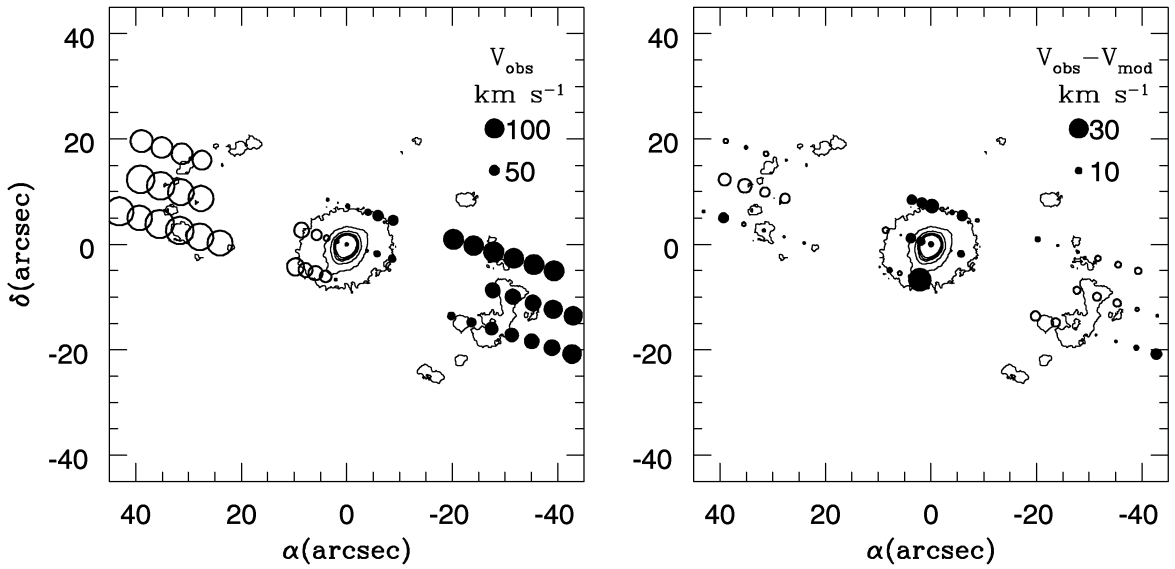

FIG. 13.—Same as Fig. 12, but for NGC 3081

km s^{-1} relative to systemic, in agreement with their value of -65 km s^{-1}. Our systemic (heliocentric) velocity of $V_{sys} = 868$ km s^{-1} and the displacement between the nucleus and the center of symmetry of the rotation curve (Fig. 16) are also in good agreement with the values found by these authors. We also point out the velocity of the point at 4″ northwest of the nucleus, which is redshifted by 25 km s^{-1} from the rotation curve at that position. This position is coincident with a high-excitation blob or shoulder observed in the [O III] images (Fig. 2), which may have been ejected from the nucleus. The redshift with respect to the rotation curve is consistent with this interpretation.

In Figures 15 and 16, where we plot the velocity curves along the position angle crossing the nucleus, we have indicated by arrows the location of the star-forming rings and inner spiral arms. It can be seen that they are all located quite close to the turnover radii. In order to verify whether the rings are located at predicted orbital resonances, we have obtained the angular velocities Ω and the Lindblad curves $\Omega \pm \kappa/2$, $\Omega \pm \kappa/4$ from the models fitted to the data (Fig. 17) for NGC 1326, NGC 3081, and NGC 7213. It should be borne in mind that the Lindblad curves have been derived from model fits to the data, rather than from the data themselves, and thus are subject to large uncertainties.

The bar in NGC 1326 has a deprojected semidiameter of 3.5 kpc. In the hypothesis that the corotation lies at the end of the bar (see, e.g., Sellwood & Wilkinson 1993), its pattern speed is $\Omega_p = 40 \pm 6$ km s^{-1} kpc^{-1}, and there are two inner Lindblad resonances (ILRs, where $\Omega_p = \Omega - \kappa/2$), at 0.15 ± 0.02 and 1.35 ± 0.15 kpc. The nuclear ring after deprojection is approximately round, with an inner radius of $\approx$0.25 kpc and an outer radius of $\approx$0.75 kpc, and is thus located between the two ILRs. A location of the nuclear ring between the two ILRs is consistent with theory (see, e.g., Piner, Stone, & Teuben 1995 and references therein)

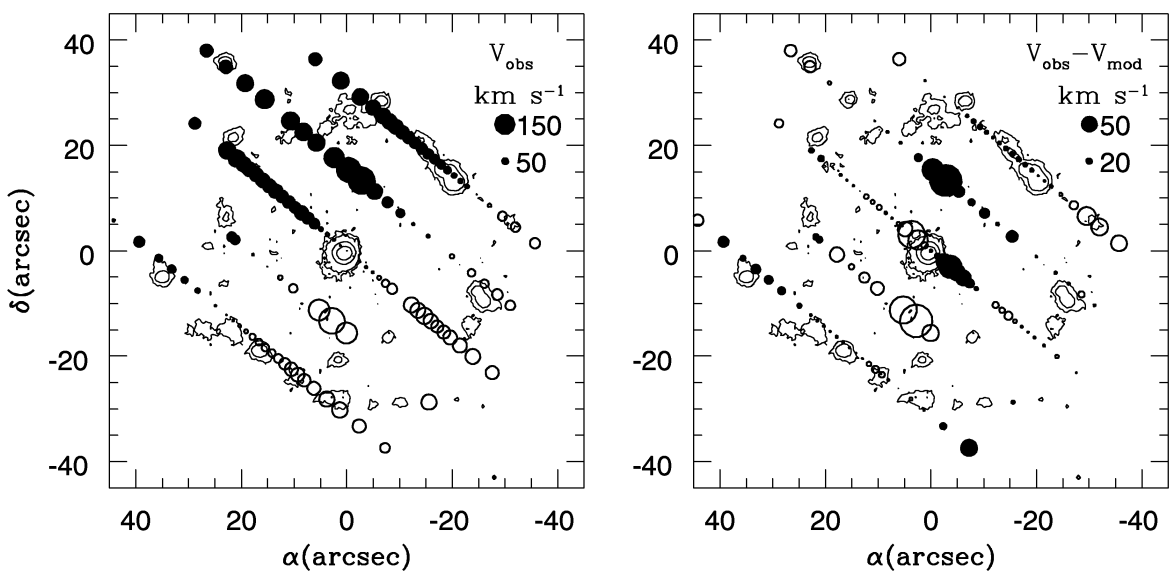

FIG. 14.—Same as Fig. 12, but for NGC 7213

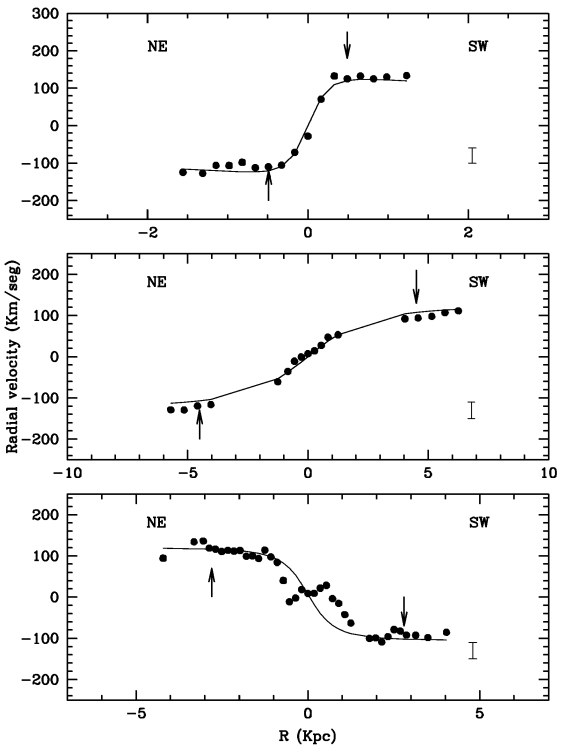

FIG. 15.—Rotation curves along the slit position through the nucleus for NGC 1326 (*top*), NGC 3081 (*middle*), and NGC 7213 (*bottom*), together with the best circular model. The locations of the star-forming rings are indicated by arrows. The error bars represent the maximum uncertainty in the individual velocity measurements (≈ 15 km s^{-1}).

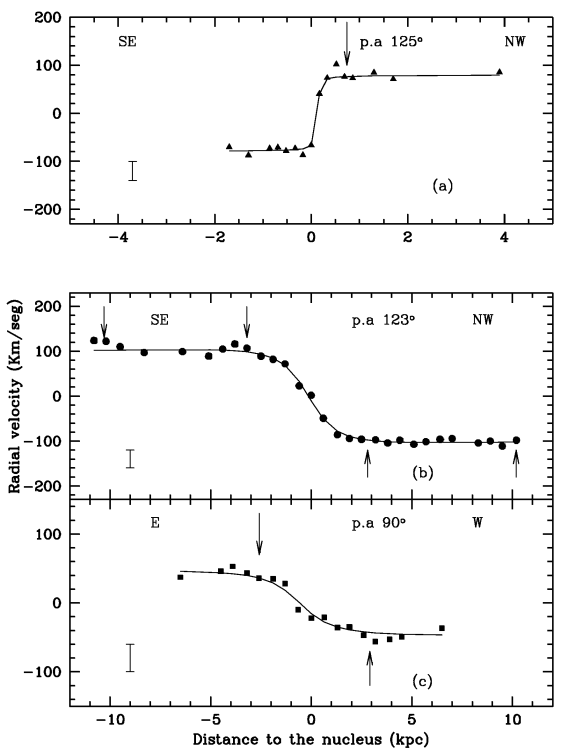

FIG. 16.—Rotation curves for NGC 1386 (*top*), NGC 1598 (*middle*), and IC 1816 (*bottom*). The locations of the H II regions (in spiral arms in at least NGC 1386 and NGC 1598) are indicated by arrows. The error bars represent the maximum uncertainty in the individual velocity measurements (≈ 15 km s^{-1}).

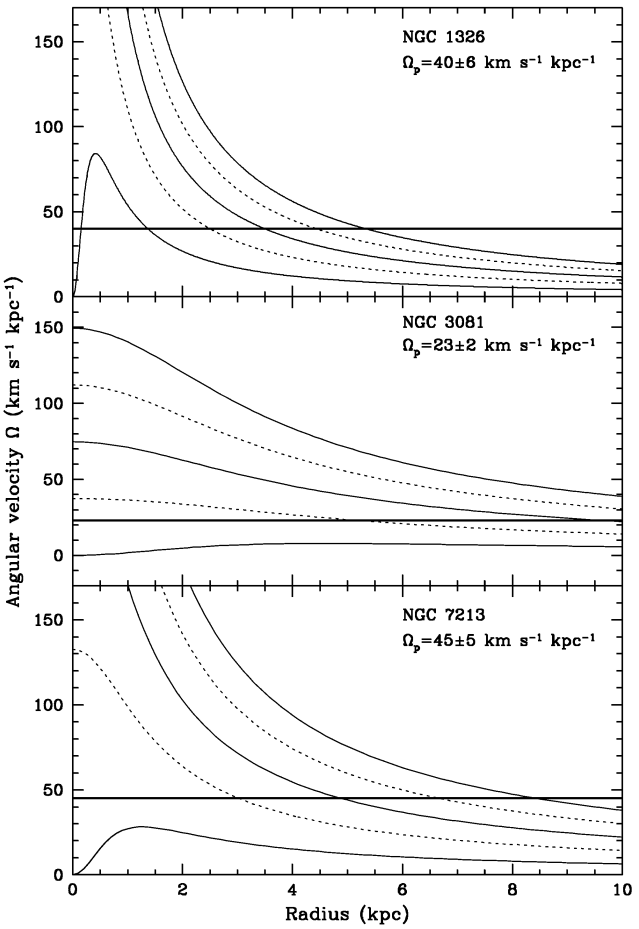

FIG. 17.—Angular velocities Ω and Lindblad curves $\Omega \pm \kappa/2$ (*solid lines*) and $\Omega \pm \kappa/4$ (*dotted lines*) obtained from the kinematic models fitted to the data. Ω_p (*heavy solid lines*) is the pattern speed of the bar in NGC 1326 and NGC 3081 and of the spiral arms in NGC 7213 (see § 5).

and previous observational works (e.g., Schommer et al. 1988 for NGC 5728; SWB for NGC 1097 and NGC 1672). Our results are also entirely consistent with those of García-Barreto et al. (1991), who also found that the nuclear ring is located between the two ILRs, although their derived pattern speed is a bit larger (~ 60 km s^{-1} kpc^{-1}).

The appearance of the rings in NGC 3081 resembles very much the particle distribution in the model of Simkin et al. (1980, their Fig. 3), where a barlike perturbation leads to the formation of an inner ring close to the end of the bar. In their model, a nuclear ring is also formed, then disappears, giving place to a nuclear bar inclined relative to the large-scale bar as is observed for the bars in NGC 3081. A *nuclear* ring of ionized gas is not seen in NGC 3081 (Fig. 4), but Buta (1990) did find a bluer continuum at the expected location ($\approx 8''$ from the nucleus). In our long-slit spectra it is also possible to detected a slightly bluer stellar population at $\approx 8''$ of the nucleus, consistent with the color obtained by Buta (1990). NGC 3081 could be between phases 3 and 5 of Simkin et al. (1980—see their Fig. 3), in which the nuclear ring is giving place to a nuclear bar. Buta (1990) suggested that the inner ring in NGC 3081 is located at the $\Omega - \kappa/4$ resonance of the bar. Under this assumption, we can use our data to derive the pattern speed of the bar from the deprojected semidiameter of the ring—5.1 kpc: $\Omega_p = 23 \pm 2$ km s^{-1} kpc^{-1}. From Figure 17, it is apparent that no ILRs

would form for such a pattern speed. However, given the caveats concerning derivation of Lindblad curves from model fits to rotation curves noted above, no firm conclusion can be reached.

In the case of NGC 7213, there is no bar and no galaxy close enough to suggest interaction. We thus speculate that the ring in this case could be formed as a result of a resonance with the spiral pattern. The radius of the ring is about 3 kpc, too large for an ILR (which usually occurs at ~ 1 kpc from the nucleus). We thus make the hypothesis that the ring is located at the resonance $\Omega_p = \Omega - \kappa/4$ and derive $\Omega_p = 45 \pm 5\ \mathrm{km\ s^{-1}\ kpc^{-1}}$.

6. EXCITATION

In all galaxies, we have found ionized gas not only at the nuclei and H II regions but also in a diffuse medium that seems to pervade the inner regions. Such emission was also observed by SWB in NGC 1097, NGC 1672, and NGC 5248 and originates in the warm ionized medium (WIM) (Rand 1995). Its detection in all sample galaxies reinforces the suggestion by Rand (1995) that it is a general feature of spiral galaxies, as well as of irregular galaxies (Hunter & Gallagher 1990).

We have used the medium-resolution spectra to construct maps of the emission-line ratios [N II]/Hα and [S II]/Hα, the observed FWHM of the emission line [N II] λ6584, and the gas densities from the ratio [S II] λ6717/λ6731. The observed $\mathrm{FWHM_{obs}}$ have been approximately corrected for the instrumental $\mathrm{FWHM_{inst}}$ through the relation $\mathrm{FWHM^2 = FWHM^2_{obs} - FWHM^2_{inst}}$. In Figures 18, 19, and 20, we show representations of the spatial variation of these quantities for NGC 1326, NGC 3081, and NGC 7213. Given the selection of spectra with fluxes of the emission lines with greater than 3–5 σ detection (§ 3), errors on the emission-line ratios are at most (for the regions with the weakest lines) $\approx 20\%$. From the measured variation of the FWHM of the sky lines along the slit, the uncertainties in the FWHM values are $\approx 15\ \mathrm{km\ s^{-1}}$. From the uncertainties on the emission-line ratios, the derived uncertainties on the density values are about 100 $\mathrm{cm^{-3}}$ for the central points

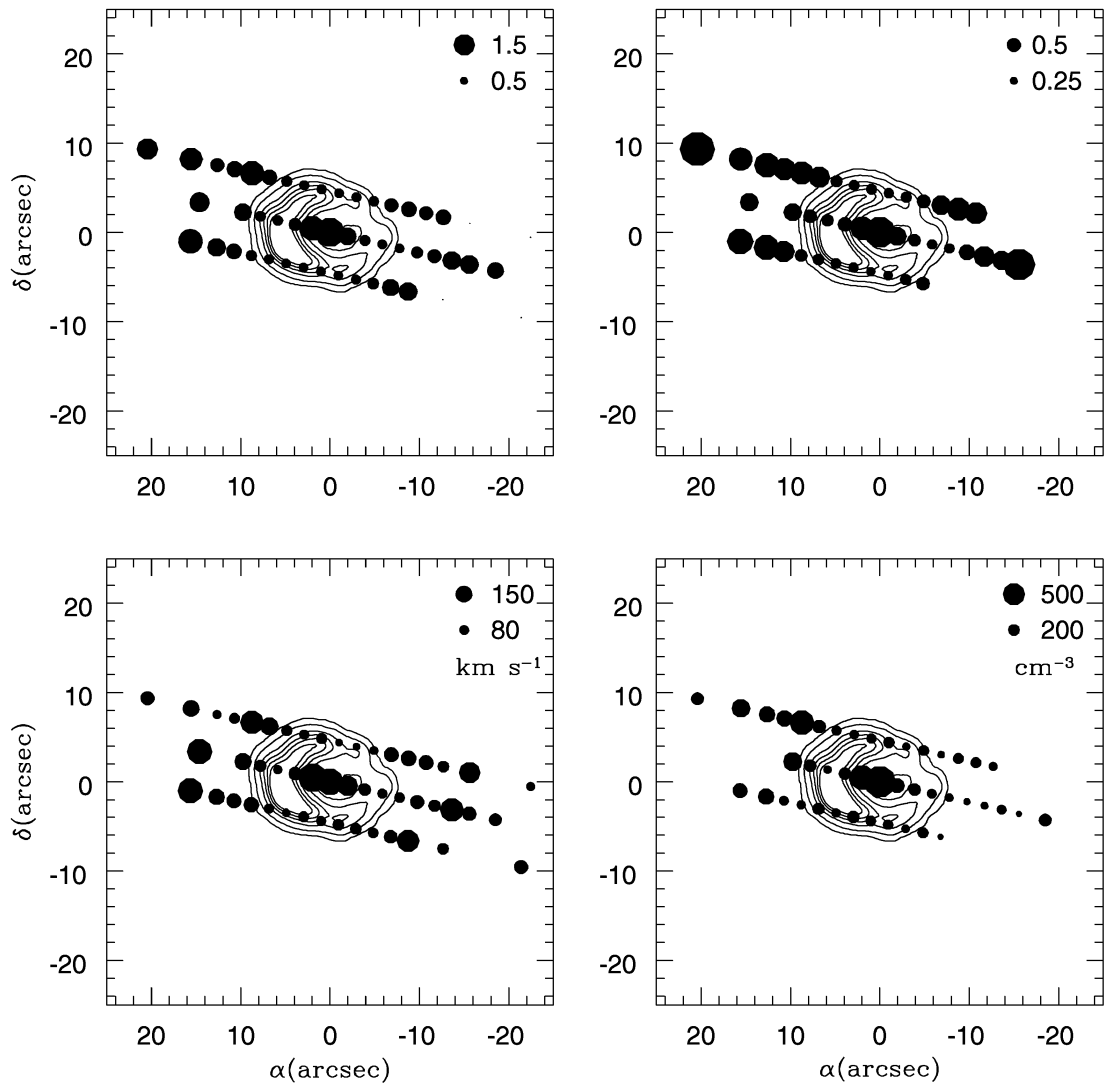

FIG. 18.—Spatial variation of emission-line ratios and FWHM. Filled circles represent the ratios [N II]/Hα (*top left*) and [S II]/Hα (*top right*), superposed on the contours of the Hα image of NGC 1326. *Bottom left*, FWHM of [N II] λ6584, corrected for the instrumental value; *bottom right*, the gas density as obtained from the [S II] λ6717/λ6731 ratio. Errors in the emission-line ratios are ≤20% (value reached at the outermost locations). Errors in the FWHM are $\leq 20\ \mathrm{km\ s^{-1}}$, while the errors in the densities are $\approx 100\ \mathrm{cm^{-3}}$.

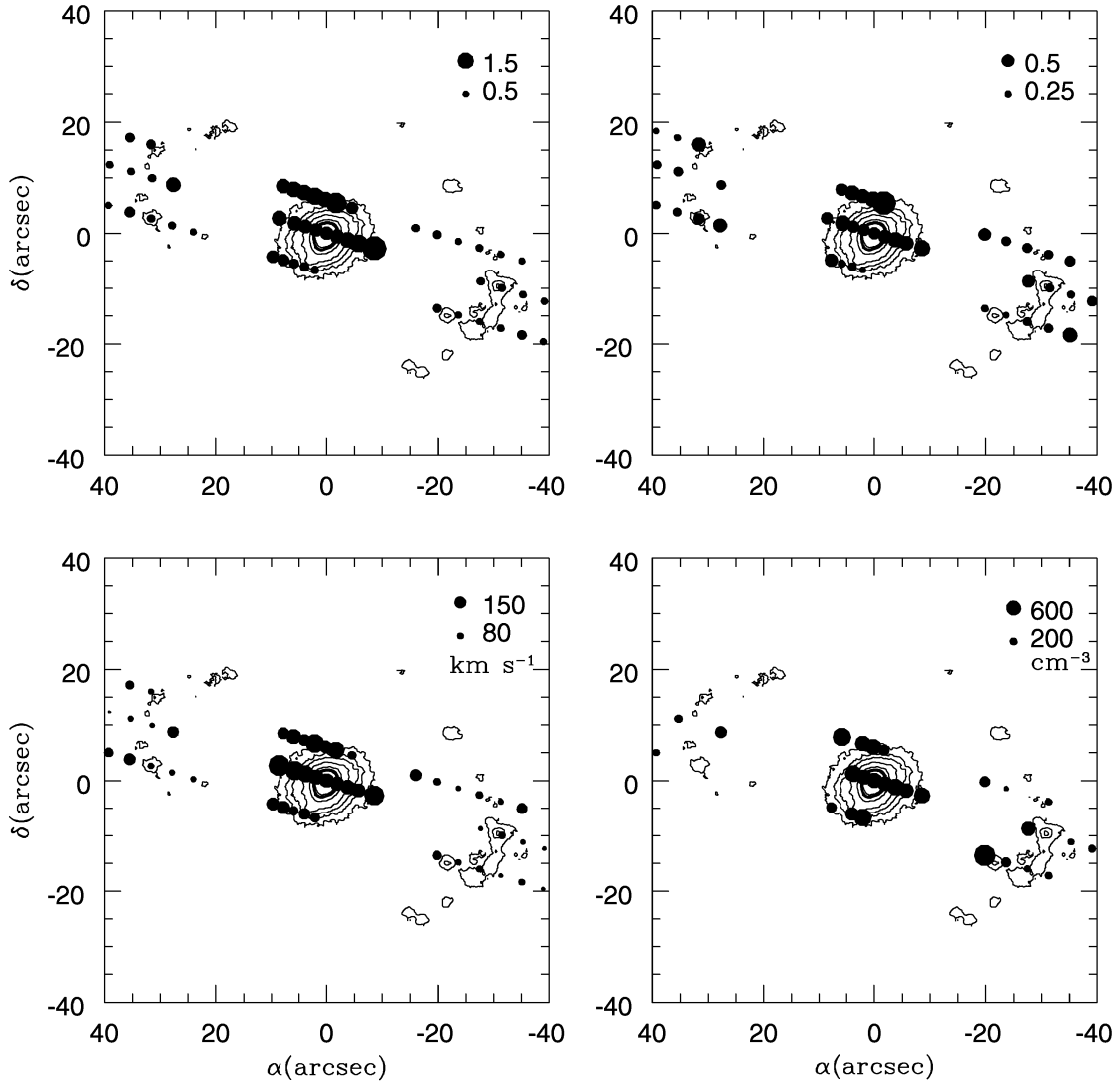

FIG. 19.—Same as Fig. 18, but for NGC 3081

and increase to about 200 cm^{-3} for the outermost locations.

Figures 18, 19, and 20 suggest a correlation between all the quantities, most notably between the emission-line ratios [N II]/Hα and [S II]/Hα and the FWHM. In order to verify a correlation between excitation and line width, we have plotted [N II]/Hα against the FWHM of [N II] λ6584 in Figure 21. The locations corresponding to the H II regions have been represented by filled triangles while the rest of the emission—the WIM—is represented by open circles.

For IC 1816, NGC 1386, and NGC 1598, we plot in Figures 22, 23, and 24 the variation of these parameters along the slit, as well as [N II]/Hα versus FWHM(λ6584).

The largest values of [N II]/Hα (up to ≈2–2.5) and [S II]/Hα (up to ≈1) are found at the nuclei and nearby regions and also outside the nuclear ring in NGC 1326, much as found for NGC 1097 and NGC 1672 (SWB). The largest ratios also correspond to the largest FWHMs and gas densities. The correlation between [N II]/Hα and the FWHM in the WIM is most clearly observed for the galaxies with data at more than one slit position, probably as a result of the larger number of data points. This correlation, as well as the corresponding density enhancements, indicates a common mechanism, most probably shocks, that compresses, ionizes, and accelerates the gas.

Figures 18, 19, and 20 show that the emission from the WIM may contaminate the emission-line fluxes of the H II regions. In order to investigate this possibility, we have measured the [N II], Hα, and [S II] fluxes per square arcsecond from the WIM just inside and outside the rings and compared these fluxes with the corresponding fluxes at the rings themselves. We have estimated the contamination of the H II region emission by assuming that the observed line fluxes represent the sum of the emission of the WIM and the H II regions. Enough measurements were possible only for the galaxies with data at more than one slit position. The degree of contamination depends on the location (mostly the distance from the nucleus) and the H II region fluxes. For NGC 1326, the ratio [N II]/Hα is increased by between 20% and 50% by the WIM emission, while [S II]/Hα is increased between 10% and 30%; for NGC 3081, [N II]/Hα is increased between 15% and 50% and [S II]/Hα by ∼10%; for NGC 7213, [N II]/Hα is increased between 20% and 40%, and [S II]/Hα is increased between 10% and 20%. We have also used the data from SWB to quantify this effect

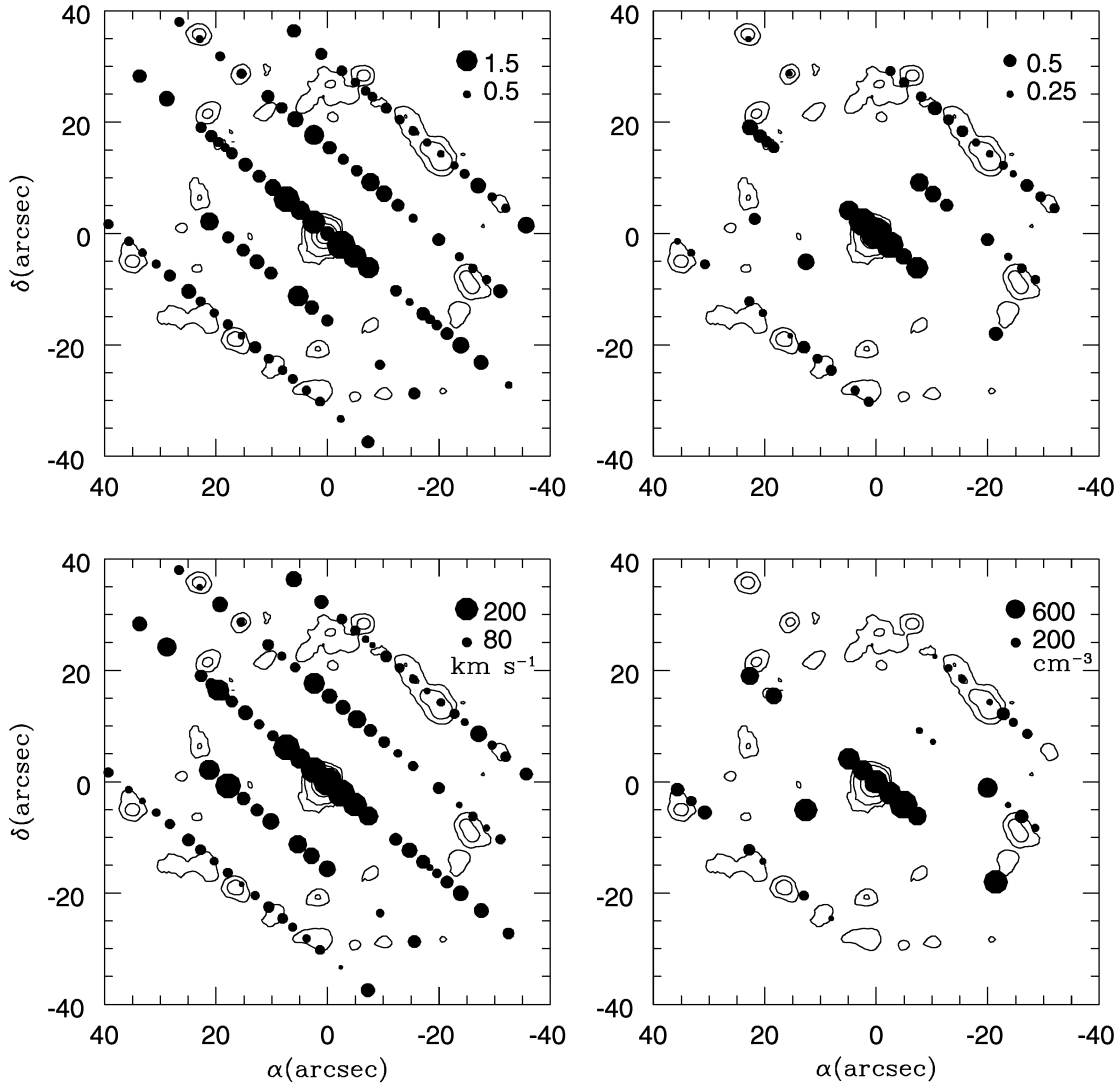

FIG. 20.—Same as Fig. 18, but for NGC 7213

in the nuclear ring of NGC 1097: the [N II]/Hα ratio might have been overestimated by ∼15%, and [S II]/Hα by ∼10%, at most, as the H II regions there are very bright.

This effect may account for previous results (e.g., Kennicutt, Keel, & Blaha 1989) that show systematically higher [N II]/Hα and [S II]/Hα ratios for H II regions near the nuclei of galaxies than for H II regions in the disks. We have directly observed and spatially separated the diffuse emission that leads to an overestimate of the above ratios in near-nuclear H II regions.

Our results are also in agreement with those of Lehnert & Heckman (1994), who proposed that the higher [N II]/Hα (and also [S II]/Hα) ratios observed in the integrated spectra of middle-to-late Hubble type galaxies can be attributed to diffuse ionized gas, either shock-ionized by supernovae and stellar winds or photoionized by diffuse starlight.

7. CHEMICAL ABUNDANCES

The reddening-corrected emission-line fluxes of the H II regions in each galaxy are listed in Table 5. The reddening-corrected line fluxes from the nuclei and the two high-excitation blobs in NGC 1386 are listed in Table 6. The reddening $E(B-V)$, listed in the last column of the tables, was obtained from the emission-line Balmer decrement Hα/Hβ, assuming an intrinsic value of 2.9. Before calculating the reddening, we corrected the Hβ fluxes for the underlying absorption from the stellar population by using the method outlined in SWB. For Hα, the corrections are negligible. Errors in most line fluxes are less than 10%. Larger errors are identified by notes in the tables.

Good signal-to-noise ratio spectra were obtained for two H II regions located at ≈8″ (≈2.6 kpc) east and west from the nucleus of IC 1816, for two H II regions in the nuclear ring of NGC 1326 at ≈6″ (≈0.5 kpc), and one H II region at 9″ (0.7 kpc) northwest in NGC 1386, for nine H II regions from 8″ to 34″ (2.5–11 kpc) both southeast and northwest from the nucleus of NGC 1598, two H II regions in the ring of NGC 3081 at ≈32″ (≈4.5 kpc), and two H II regions in the ring of NGC 7213 at ≈27″ (≈3.0 kpc). The line fluxes from Table 5 were used to calculate the gaseous oxygen and nitrogen abundances of the H II regions, using the method and assumptions described in SWB.

The values for the gas temperature, oxygen abundance expressed as log (O/H) + 12 (where O/H is the number ratio between the oxygen and hydrogen abundances), and log (N/O) (where N/O is the number ratio between the

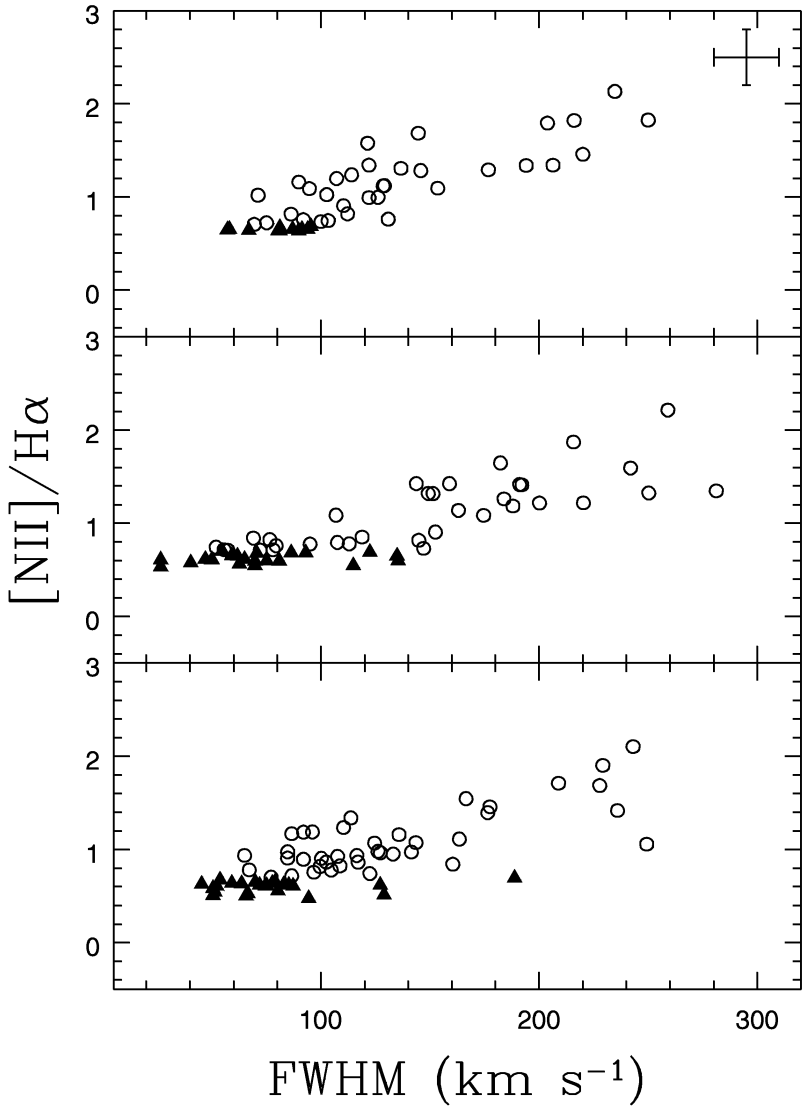

FIG. 21.—Emission-line ratio [N II]/Hα plotted as a function of the FWHM of [N II] λ6584, corrected for the instrumental FWHM. *Top*, NGC 1326; *middle*, NGC 3081; *bottom*, NGC 7213. Circles represent the diffuse emission, and triangles represent the H II regions. The error bars correspond to the outermost locations and represent the maximum errors in the above quantities.

nitrogen and oxygen abundances) are listed in Table 7. The uncertainties on these quantities have been calculated from the errors in the emission-line fluxes. For reference, the adopted solar values are log (O/H) + 12 = 8.91 and log (N/O) = −0.93 (Aller 1987; Grevesse 1984).

The derived temperatures and N and O abundances may be affected by the contamination by the WIM. Using the results for NGC 1326, NGC 3081, and NGC 7213 from the previous section, we have corrected these values under the assumption that the flux of the [O II] λ3727 line is increased by the same factor as the flux of the [N II] λλ6548, 6584 lines. This is due to the fact that O^+ and N^+ have similar ionization potentials, and any additional ionization source in the WIM will increase the emission from both ions. We also show, in parentheses, the values obtained before the correction for the contamination by the WIM. It can be concluded that the contamination by the WIM may lead to an overestimate of the temperature of ∼500 K, an underestimate of the O abundance by ∼0.1 dex, and an overestimate of the N/O ratio by up to ≈0.1 dex.

7.1. *Discussion*

What can we say about the gas abundances at the nuclei from the results obtained for the H II regions?

Only for NGC 1598, which has nine H II regions, was it possible to derive a radial abundance gradient from the data. In Figure 25, we show the data together with a linear fit with slope -0.06 ± 0.01 dex kpc^{-1}, which implies a central log (O/H) + 12 = 9.24 ± 0.07. This gradient and central oxygen abundance of approximately 2 times solar are well within the range observed for galaxies of the same morphological type as NGC 1598 (Vila-Costas & Edmunds 1992, hereafter VE92).

NGC 1326 and NGC 1386 have H II regions only a fraction of a kiloparsec away from the nucleus, and the results suggest that the nuclear abundance is close to solar. A solar central abundance is at the lower limit of the range observed by VE92 for normal Sa galaxies. For IC 1816, the O/H is just above solar at 2–3 kpc from the nucleus. From VE92, it can be concluded that such a value is also within

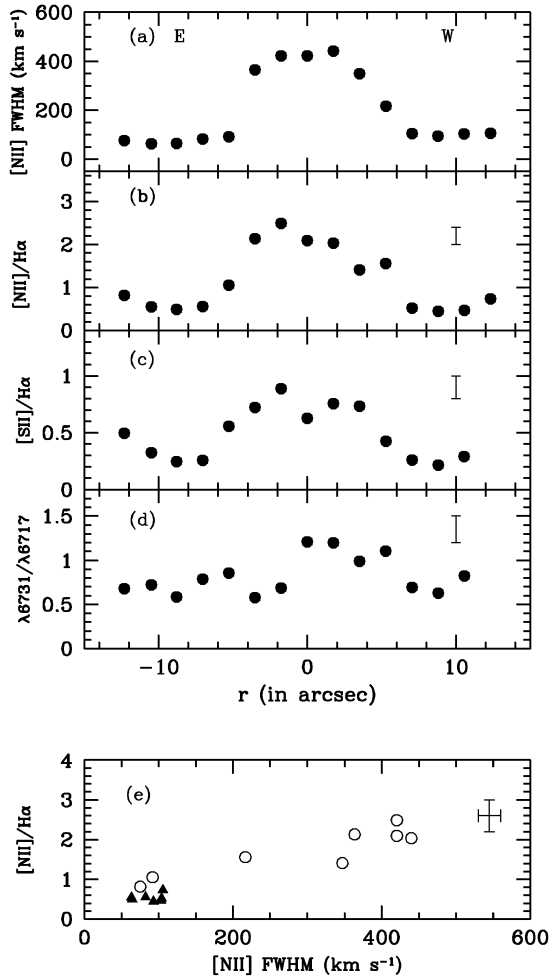

FIG. 22.—*Top to bottom*: FWHM of [N II] λ6584, corrected for the instrumental FWHM, and the emission-line ratios [N II]/Hα, [S II]/Hα, and [S II] λ6731/λ6717 plotted as a function of distance from the nucleus for IC 1816. The lower panel shows [N II]/Hα plotted against [N II] FWHM; open circles represent the diffuse emission, and triangles represent the H II regions. The error bars correspond to the outermost locations and represent the maximum errors in the above quantities.

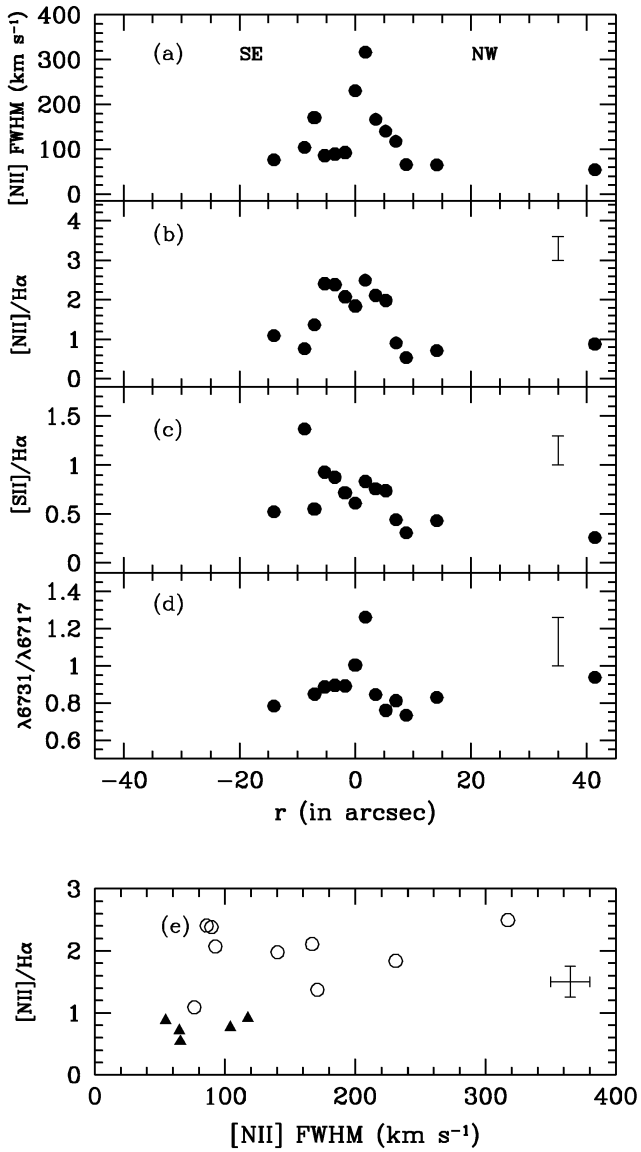

FIG. 23.—Same as Fig. 22, but for NGC 1386

the range observed for normal galaxies. Adopting a typical gradient for its morphological type of -0.05 dex kpc^{-1}, we obtain a nuclear abundance approximately 2 times solar. For NGC 3081, the two H II regions at 4.5 kpc from the nucleus have just over solar oxygen abundances, suggesting an oversolar abundance for the nucleus. For NGC 7213, the oxygen abundance for the ring is about solar. If we adopt the same typical gradient as above, the extrapolated nuclear abundance is just over solar, which is within the range of values obtained for normal galaxies with the same morphological type and absolute magnitude (VE92; Kennicutt et al. 1993).

Figure 25 also shows the dependence of the logarithm of the N/O ratio on the oxygen abundance for NGC 1598. The solid line is a linear fit to the data, which agrees very well with the dashed line, representing a model by Vila-Costas & Edmunds (1993) in which the nitrogen abundance is dominated by secondary processes, and which is found to describe the behavior of normal metal-rich galaxies. The extrapolated nuclear N/O ratio is about 2 times solar, thus corresponding to a nitrogen abundance of ≈4 times solar. For the other galaxies, the N/O ratios as a function of O/H approximately agree with Vila-Costas & Edmunds' (1993) relation for NGC 3081 and NGC 7213 and are about 0.15 dex above the relation for IC 1816, NGC 1326, and NGC 1386. The extrapolated nuclear values for the nitrogen abundances are approximately 2 times solar for NGC 1326, NGC 1386, and NGC 7213 and 4 times solar for IC 1816 and NGC 3081.

8. SUMMARY AND CONCLUSIONS

We have investigated the gas kinematics, excitation, and chemical abundance of six galaxies with active galactic nuclei and H II regions in rings or spirals close to the nuclei.

Narrowband Hα images reveal a nuclear ring in NGC 1326, inner rings in NGC 3081 and NGC 7213, and spiral arms in NGC 1386 and NGC 1598. [O III] λ5007 emission is extended in NGC 1386, showing two high-excitation knots, one at ≈4–5″ and the other at ≈40″ from the nucleus along P.A. −11°. In NGC 3081, both narrowband images—Hα and [O III] λ5007—show emission from a compact region elongated perpendicular to the large-scale bar, with extent similar to that of the nuclear bar. No

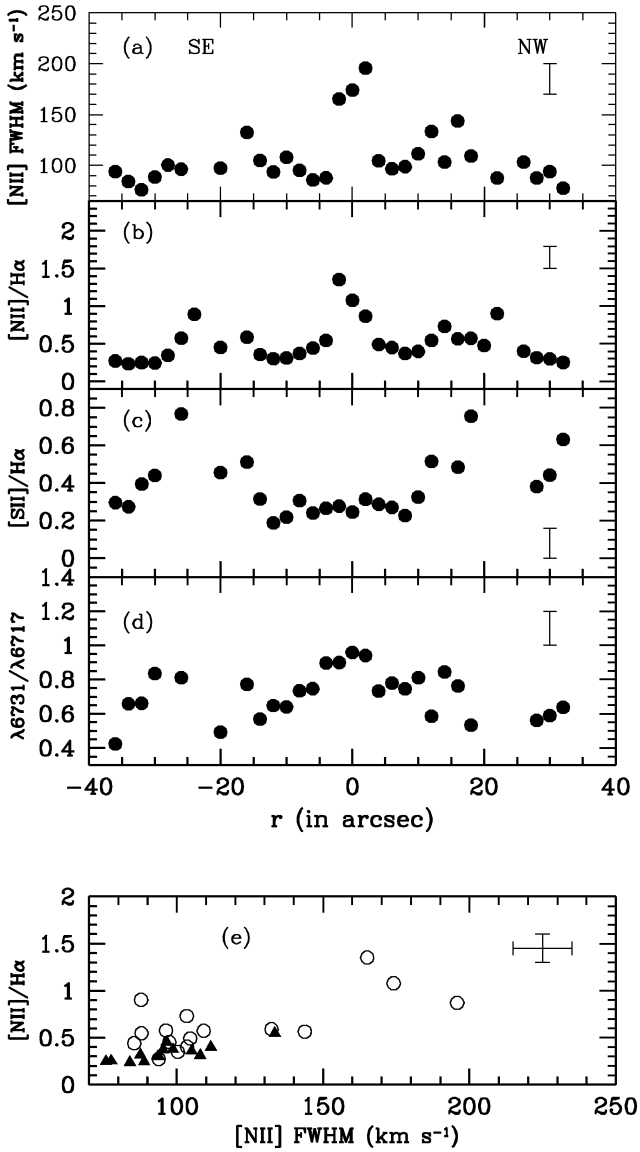

FIG. 24.—Same as Fig. 22, but for NGC 1598

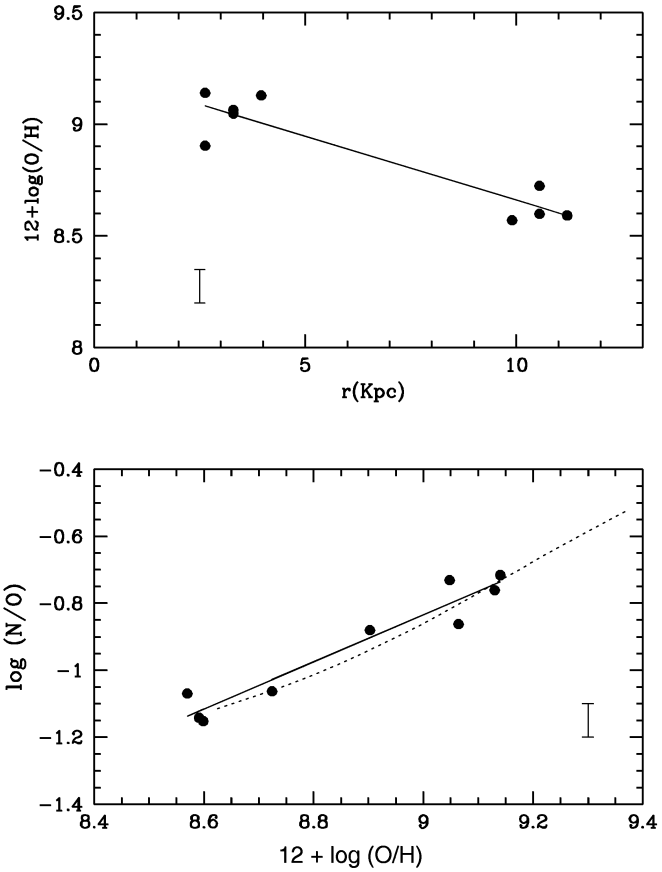

FIG. 25.—*Top*: Oxygen abundance, in units of 12 + log (O/H), as a function of radial distance from the nucleus of NGC 1598, plotted together with a linear fit to the data. *Bottom*: The log (N/O) ratio as a function of 12 + log (O/H). The solid line shows the fit to the NGC 1598 data, and the dotted line is the Vila-Costas & Edmunds (1992) model.

gaseous nuclear ring was observed in NGC 3081 at the location of the blue continuum ring found by Buta (1990). An inner spiral structure is revealed by continuum color images of NGC 7213.

The gaseous velocity fields are generally well described by a model involving circular rotation. For NGC 7213, there are systematic residuals of up to $\approx$100 km s^{-1}, indicating noncircular motions. The radii at which the rotation curve turns over in NGC 1326 and NGC 1386 are unusually small (0.30 and 0.11 kpc, respectively) in comparison with normal galaxies of similar luminosity and morphological type (1–2 kpc), indicating an unusual central mass concentration. The locations of the rings are consistent with orbital resonances. In NGC 1326, the nuclear ring is located at the turnover of the rotation curve and probably between the two ILRs. In all other galaxies, the H II regions are located close to, but somewhat beyond, the turnover of the rotation curves. In NGC 3081 and NGC 7213, the inner rings may be located at the $\Omega - \kappa/4$ resonance.

Besides the gaseous emission from the nuclei and H II regions, diffuse emission—a warm ionized medium (WIM)—is found to pervade the inner regions of all six galaxies. The WIM is characterized by high values of the [N II]/Hα and [S II]/Hα ratios, the FWHM of the [N II] λ6584 line, and gas density. These quantities are correlated, consistent with ionization by shocks. The WIM contaminates emission from near-nuclear H II regions, leading to increased [N II]/Hα (from 10% to 50%) and [S II]/Hα (from 5% to 20%) ratios. This effect has been noted in previous works via diagnostic diagrams for H II regions close to galactic nuclei (e.g., Kennicutt et al. 1989), but the WIM is spatially resolved from the H II regions in our observations.

Oxygen and nitrogen gaseous abundances were determined for 18 H II regions. For the LINER NGC 1598, the gradient in the oxygen abundance is -0.06 ± 0.01 dex kpc^{-1}, and the extrapolated central value is 12 + log (O/H) = 9.24 ± 0.07, which are similar to those of "normal" galaxies with the same morphological type and absolute magnitude. The value of log (N/O) was found to correlate with 12 + log (O/H) in a manner identical to H II regions in normal galaxies, a relationship that is well described by a chemical evolution model in which nitrogen synthesis is mostly secondary. The extrapolated nuclear nitrogen abundance is 4 times solar.

For the other galaxies, it was not possible to derive abundance gradients, but assuming a gradient typical of galaxies

TABLE 5

H II Regions' Reddening-corrected Line Fluxes

Location (kpc)	λ3727	Hβ	λ5007	λ6300	Hα	λ6584	λ6717	λ6732	$E(B-V)$
IC 1816:									
2.91 W	3.8	2.9	0.9[a]	...	8.5	3.4	1.4	0.8[b]	0.25
2.58 E	2.0	2.2[c]	0.8[b]	...	6.3	2.7	1.0	0.7[b]	0.18
NGC 1326:									
0.49 SW.....	37.3	18.7	9.5	...	54.0	31.4	13.2	10.1	0.58
0.49 NE	47.4	35.4	11.6	...	101.9	52.4	20.3	15.2	0.27
NGC 1386:									
0.74 NW	11.0	7.3	2.8[b]	...	22.0	9.0	3.7	2.8	0.55
NGC 1598:									
2.54 NW	3.0	2.9	0.4[b]	0.3	8.5	3.4	1.1	0.7	0.41
3.18 NW	3.2[c]	2.8	0.9[b]	0.2	8.5	3.1	1.3	0.7[b]	0.55
10.18 NW.....	0.24	0.13	0.08[b]	...	0.34	0.09[b]	0.09[c]	0.05[a]	0.0
2.54 SE.....	2.8	1.7	0.2[a]	...	5.0	1.8	0.7	0.5[b]	0.47
3.18 SE.....	3.2[c]	2.6	0.6[b]	0.2	7.7	2.4	0.9	0.6	0.36
3.82 SE.....	1.4	1.6	0.3[c]	0.2	4.6	1.5	0.6	0.4	0.13
9.54 SE.....	1.7	0.5	0.5[b]	...	1.4	0.4	0.4[a]	0.2	0.42
10.18 SE	4.2	1.2	1.5	0.1[c]	3.5	0.8	0.7	0.4	0.27
10.81 SE	4.1	1.1	1.5	...	3.3	0.8	0.6	0.4	0.22
NGC 3081:									
4.50 SW.....	9.2	5.9	1.2	...	16.9	7.1	1.7	1.2	0.43
4.50 NE	1.4[c]	1.4	0.1[a]	...	3.9	1.7	0.7[c]	0.3[c]	0.12
NGC 7213:[d]									
2.77 NW	24.5	11.9	3.0	...	35.2	17.9	7.5	4.9	0.26
3.01 NW	3.1	1.3	0.4[c]	...	4.0	2.4	1.2	0.7[c]	0.0

Note.—In units of 10^{-15} ergs cm^{-2} s^{-1}.
[a] Error between 30% and 50%.
[b] Error between 10% and 20%.
[c] Error between 20% and 30%.
[d] Only relative fluxes for NGC 7213, as a result of clouds during observation of flux standard.

of the same morphological type and absolute magnitude, we obtain nuclear O/H and N/O values ranging from solar to 2 times solar. The final nitrogen abundances obtained for the nuclei range from 2 to 4 times solar, which agree well with the values obtained previously for the NLRs of Seyfert galaxies and LINERs (Storchi-Bergmann & Pastoriza 1989, 1990). Nevertheless, the nuclear values are within the range observed for normal galaxies and do not support abnormal chemical processing of the nuclear gas in active galaxies.

This work was partially supported by the Brazilian institutions FINEp, FAPERGS, and CNPq and by NASA through grants NAGW-3268 and NAG 8-1027. We acknowledge fruitful discussions with H. Dottori and useful suggestions from L. Sparke and J. Sellwood and J. Steiner, from an anonymous referee and the editor, G. Bothun, which helped to improve the paper. We also thank H. Fraquelli for help with the figures.

TABLE 6

Nuclear and High-Excitation Reddening-corrected Line Fluxes

Galaxy	λ3426	λ3727	λ3869	λ4340	λ4363	λ4686	Hβ	λ5007	λ5200	λ6300	Hα	λ6584	λ6717	λ6732	$E(B-V)$
IC 1816	...	52.0	42.0	14.0	11.0	8.1	26.7	366.7	5.2	32.0	78.1	141.7	31.4	31.4	0.14
NGC 1326	...	426.1	...	...	...	...	32.3	65.2	...	...	93.0	143.6	58.5	58.8	1.12
NGC 1386	...	263.5	134.0	...	83.8	121.9	1486.8	...	47.8	366.0	467.0	103.7	104.1	0.62	...
0.49 kpc SE	...	0.3[a]	...	...	...	...	0.5[a]	0.8	...	...	1.5	1.0	0.4[a]	0.3[a]	0.45
0.49 kpc NW.....	...	2.2	...	...	...	...	1.9	4.6	...	...	5.6	4.8	1.5	1.0	0.44
3.28 kpc NW.....	...	0.5	...	...	...	...	0.2[a]	1.6	...	...	0.6	0.4	0.1[b]	0.1[b]	0.0
NGC 1598	...	11.2	...	...	...	17.2	30.7	4.0	1.6[c]	51.6	61.5	6.5	...	4.8	0.56
NGC 3081	19.7	18.1	10.1	4.9	4.5	5.2	11.8	136.8	...	2.2	35.4	33.1	9.0	7.0	0.29

Note.—In units of 10^{-15} ergs cm^{-2} s^{-1}.
[a] Error between 10% and 20%.
[b] Error between 30% and 50%.
[c] Error between 20% and 30%.

TABLE 7

H II Regions' Oxygen and Nitrogen Abundances

Location (kpc)	T_e (K)	log (O/H) + 12	log (N/O)
IC 1816:			
2.91 W	5000 ± 250	9.01 ± 0.09	−0.76 ± 0.04
2.58 E	4550 ± 150	9.05 ± 0.03	−0.63 ± 0.03
NGC 1326:			
0.49 SW.....	5400 ± 200 (6150)	8.89 ± 0.04 (8.76)	−0.74 ± 0.02 (−0.66)
0.49 NE.....	4500 ± 200 (5050)	9.08 ± 0.03 (8.95)	−0.72 ± 0.02 (−0.66)
NGC 1386:			
0.74 NW.....	5350 ± 200	8.89 ± 0.04	−0.75 ± 0.03
NGC 1598:			
2.54 NW.....	4350 ± 100	9.14 ± 0.02	−0.72 ± 0.02
3.18 NW.....	4750 ± 500	9.05 ± 0.12	−0.73 ± 0.05
10.18 NW.....	6250 ± 200	8.72 ± 0.04	−1.00 ± 0.07
2.54 SE.....	5100 ± 300	8.90 ± 0.04	−0.88 ± 0.03
3.18 SE.....	4700 ± 500	9.06 ± 0.11	−0.86 ± 0.05
3.82 SE.....	4200 ± 200	9.22 ± 0.03	−0.78 ± 0.05
9.54 SE.....	7850 ± 200	8.59 ± 0.02	−1.07 ± 0.04
10.18 SE	8100 ± 200	8.60 ± 0.02	−1.15 ± 0.02
10.81 SE	8300 ± 200	8.56 ± 0.01	−1.12 ± 0.02
NGC 3081:			
4.50 SW.....	4700 ± 150 (5100)	9.00 ± 0.01 (8.92)	−0.85 ± 0.02 (−0.80)
4.50 NE.....	3800 ± 150 (4200)	9.14 ± 0.02 (9.05)	−0.78 ± 0.01 (0.72)
NGC 7213:			
2.77 NW.....	5300 ± 100 (5800)	8.89 ± 0.01 (8.81)	−0.80 ± 0.01 (−0.75)
3.01 NW.....	5400 ± 100 (6300)	8.88 ± 0.02 (8.74)	−0.77 ± 0.02 (−0.68)

Note.—Values in parentheses are not corrected for the contribution of diffuse emission; see § 7.

REFERENCES

Aller, L. H. 1987, in Spectroscopy of Astrophysical Plasmas, ed. A. Dalgarno & D. Layzer (Cambridge: Cambridge Univ. Press), 89
Appenzeller, I., & Östreicher, R. 1988, AJ, 95, 45
Bertola, F., Bettoni, D., Danziger, J., Sadler, E., Sparke, L., & de Zeeuw, T. 1991, ApJ, 373, 369
Buta, R. 1990, ApJ, 351, 62
Buta, R., & Crocker, D. A. 1993, AJ, 105, 1344
Durret, F., & Bergeron, J. 1986, A&A, 156, 51
Filippenko, A. V., & Halpern, J. P. 1984, ApJ, 285, 458
García-Barreto, J. A., Dettmar, R.-J., Combes, F., Gerin, M., & Koribalski, B. 1991, Rev. Mexicana Astron. Astrofis., 22, 197
Genzel, R., Weitzel, L., Tacconi-Garman, L. E., Blietz, M., Cameron, M., Krabbe, A., Lutz, D., & Sternberg, A. 1995, ApJ, 444, 129
Grevesse, N. 1984, in Frontiers of Astronomy and Astrophysics, Seventh European Regional Astron. Meeting, ed. R. Pallavicini (Florence: Italian Astron. Soc.), 71
Hawarden, T. G., Longmore, A. J., Cannon, R. D., & Allen, D. A. 1979, MNRAS, 186, 495
Hunter, D. A., & Gallagher, J. S., III. 1990, ApJ, 362, 480
Kennicutt, R. C., Keel, W. C., & Blaha, C. A. 1989, AJ, 97, 1022
Kennicutt, R. C., Oey, M. S., Zaritsky, D., & Huchra, J. P. 1993, Rev. Mexicana Astron. Astrofis., 27, 21
Lauberts, A. L., & Valentijn, E. A. 1989, The Surface Photometry Catalogue of the ESO-Uppsala Galaxies (Garching: ESO)
Lehnert, M., & Heckman, T. M. 1994, ApJ, 426, L27
Maia, M. A. G., da Costa, L. N., Willmer, C., Pellegrini, P. S., & Rité, C. 1987, AJ, 93, 546
Phillips, M. M., Charles, P. A., & Baldwin, J. A. 1983, ApJ, 266, 485
Phillips, M. M., Pagel, B. E. J., Edmunds, M. G., & Diaz, A. 1984, MNRAS, 210, 701
Piner, B. G., Stone, J. M., & Teuben, P. J. 1995, ApJ, 449, 508
Pogge, R. W. 1989, ApJ, 345, 730
Rand, R. J. 1995, in Gas Disks in Galaxies, ed. J. M. van der Hulst (Dordrecht: Kluwer), in press
Rubin, V. C., Burstein, D., Ford, W. K., Jr., & Thonnard, N. 1985, ApJ, 289, 81
Sandage, A., & Tammann, G. A. 1987, A Revised Shapley-Ames Catalog of Bright Galaxies (2d ed.; Washington: Carnegie Inst. Washington)
Schmitt, H. R., Storchi-Bergmann, T., & Baldwin, J. A. 1994, ApJ, 423, 237
Schommer, R. A., Caldwell, N., Wilson, A. S., Baldwin, J. A., Phillips, M. M., Williams, T. B., & Turtle, A. J. 1988, ApJ, 324, 154
Sellwood, J., & Wilkinson, A. 1993, Rep. Prog. Phys., 56, 173
Simkin, S. M., Su, H. J., & Schwarz, M. P. 1980, ApJ, 237, 404
Storchi-Bergmann, T. 1991, MNRAS, 249, 404
Storchi-Bergmann, T., Bica, E., & Pastoriza, M. G. 1990, MNRAS, 245, 749
Storchi-Bergmann, T., & Pastoriza, M. 1989, ApJ, 347, 195
———. 1990, PASP, 102, 1359
Storchi-Bergmann, T., Wilson, A. S., & Baldwin, J. A. 1992, ApJ, 396, 45
———. 1996, ApJ, 460, 252 (SWB)
Tully, R. B. 1988, Nearby Galaxies Catalog (Cambridge: Cambridge University Press)
Véron, P. 1981, A&A, 100, 12
Véron-Cetty, M.-P., & Véron, P. 1986, A&AS, 66, 335
Vila-Costas, M. B., & Edmunds, M. G. 1992, MNRAS, 259, 121 (VE92)
———. 1993, MNRAS, 265, 199
Weaver, K. A., Wilson, A. S., & Baldwin, J. A. 1991, ApJ, 366, 50
Whittle, M. 1985, MNRAS, 216, 817
Wilson, A. S., Helfer, T. T., Haniff, C. A., & Ward, M. J. 1991, ApJ, 381, 79